

# Redefining the Electron (Part 3):

## The Implications for EMR and Gravity

by

**David Johnson**

David.Johnson.Pivot@gmail.com

### Table of Contents (Active hyperlinks by Chapter heading)

Abstract .....	2
Photons, Energy Transfer and Spectral Lines .....	2
Light Refraction .....	8
Constructive and Destructive Interference .....	9
The Photoelectric Effect .....	13
Electron-Positron Annihilation .....	15
Semiconductors, P-N Junctions and Holes .....	16
Plasma and Cosmic Radiation.....	21
Spin and the Orbital Nuclear Model.....	22
The Pull of Gravity .....	23
Issues Related to Quark and Nucleon Size and Mass .....	25
Conclusions .....	27
Acknowledgements and References .....	28
Appendix: Micro and Radio Waves .....	29

### Figures

<i>Figure 1: A Photon as a Helical Solenoid</i> .....	2
<i>Figure 2: Nucleon Quark Structure</i> .....	3
<i>Figure 3: Photon Creation/Emission and Capture/Re-Emission</i> .....	4
<i>Figure 4: Emission Spectra for Common Element Groupings</i> .....	5
<i>Figure 5: Absorption and Re-Emission Spectra</i> .....	5
<i>Figure 6: Unpolarised Photon Electromagnetic Fields</i> .....	6
<i>Figure 7: Optic Vortex and Linear, Circular and Polarised Light Forms</i> .....	7
<i>Figure 8: Reflection of Circular Polarised Light</i> .....	8
<i>Figure 9: Light Refraction</i> .....	8
<i>Figure 10: Michelson Interferometer setup: parallel merged beams</i> .....	9
<i>Figure 11: Michelson Interferometer Interference Patterns</i> .....	9
<i>Figure 12: Surface Plasmons and Far-Field Scatter Effects</i> .....	10
<i>Figure 13: 2-Slit Experiment for Light</i> .....	11
<i>Figure 14: 2-Slit Electron Electromagnetic Deflection and Distribution Pattern</i> .....	12
<i>Figure 15: The Photoelectric Effect</i> .....	13
<i>Figure 16: Stopping Voltages to the Photoelectric Effect by Element</i> .....	14
<i>Figure 17: Pair Production</i> .....	14
<i>Figure 18: Electron-Positron Annihilation</i> .....	15
<i>Figure 19: The P-N Junction</i> .....	16
<i>Figure 20: Silicon Atom and Wafer Structure and Orientation</i> .....	17
<i>Figure 21: The Structure of the Dopants</i> .....	18
<i>Figure 22: Effects of Dopant Ionisation</i> .....	19
<i>Figure 23: Boundary Effects and Forward/Reverse Bias Effects</i> .....	20
<i>Figure 24: Plasma Temperature/Density Distribution</i> .....	21
<i>Figure 25: The Stern–Gerlach Experiment Setup</i> .....	22
<i>Figure 26: The Stern–Gerlach Experiment Deflection Pattern</i> .....	23
<i>Figure 27: Model for Earth’s Gravity</i> .....	24
<i>Figure 28: Helium-4 and T-form Nucleons</i> .....	26
<i>Figure 29: Electron and Positron Electromagnetic Field Patterns</i> .....	29
<i>Figure 30: Man-Made Micro and Radio Waves</i> .....	29
<i>Figure 31: Electromagnetic Field Patterns for a Dipolar Antenna</i> .....	30

April 2019

# Abstract

The **Spin Torus Energy Model (STEM)** was introduced in [Part 1 of the 'Redefining the Electron'](#) series to define the structure of electrons and positrons so as to explain the nature of electric and magnetic fields, electric current generation from battery and induction sources, capacitor charge and discharge, and superconductivity. STEM was extended in [Part 2](#) to define a structure Preons, quarks and nucleons and to explore the nuclear structure of atoms. The atomic model developed provides explanations for the physical characteristics and different allotropic forms of elements in the Periodic Table, their various bonding geometries, and for electron capture and beta decay.

This is the third and final paper which provides a STEM explanation for the particle-wave nature of EMR, spectral line emission and absorption, the photo-electric effect, the Compton effect, P-N semiconductors, electron pair generation and annihilation, plasma, cosmic radiation and Gravity.

Part 3 also provides a summary of physics and chemistry related phenomena addressed by STEM in parts 1 to 3 plus an appendix that addresses the special nature of micro and radio waves.

## Photons, Energy Transfer and Spectral Lines

The wave nature of EMR has allowed the allocation of wavelengths for [the complete EMR spectrum from Gamma to long radio wave](#), and a detailed colour map of EMR by wavelength in the visible light range. From the colour of light, its wavelength can thus be determined and, using Planck's constant and the speed of light, the formula  $E=hc/\lambda$  allows the corresponding energy of photons to be calculated.

STEM considers the photon to be particle formed by concentrated energy travelling as a helical solenoid (see figure 1). Thus photons have wave-like characteristics, which aligns with the Quantum Mechanic's particle-wave duality concept as supported by the Schrödinger and Dirac equations, and is not far removed from the vibrating string concept of String theory. STEM can provide a simple feasible mechanism for the generation and emission of photons that is considerably different to the electron orbit-jumping mechanism supported by the orbital nuclear model approach of conventional Science.

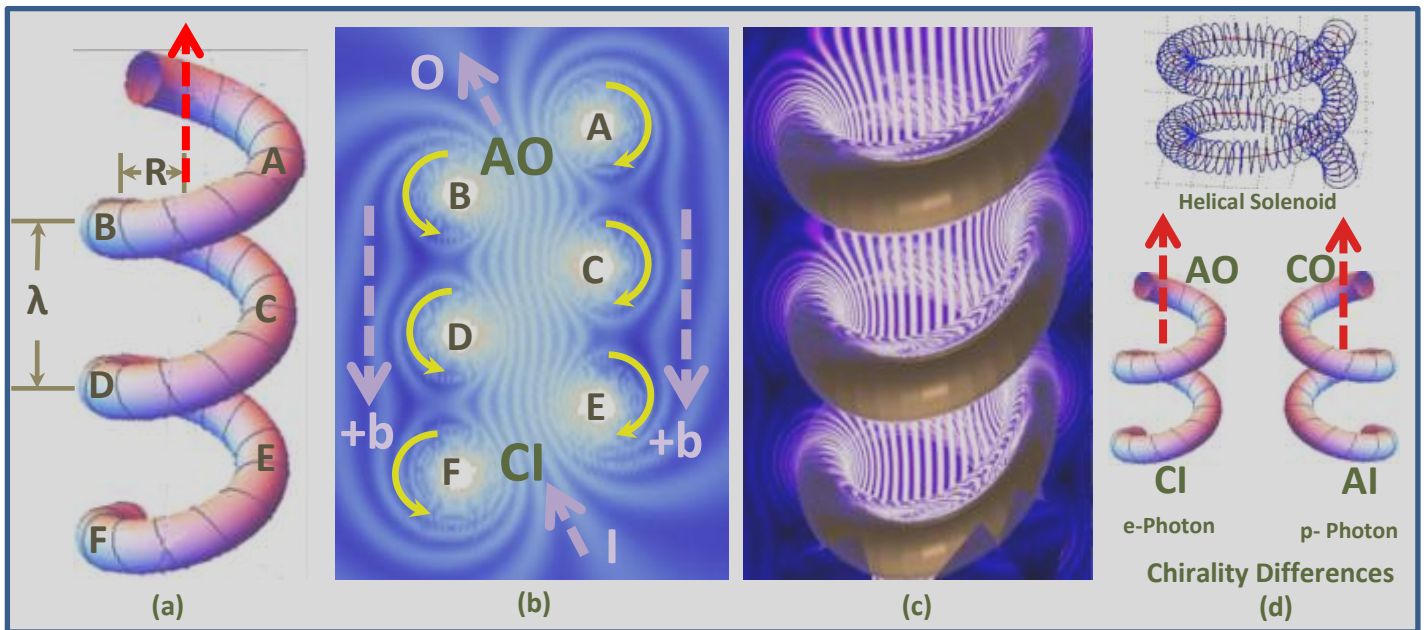


**Figure 1: A Photon as a Helical Solenoid**

Oliver Consa, in his 2018 paper ['Helical Solenoid Model of the Electron'](#), uses the helical solenoid model for the electron and to preons in a later paper. STEM, however, contends that the helical solenoid structure is specific to the photon, with the spin-toroidal structure being more appropriate to the electron, positron and preon (CES) as covered in parts 1 and 2 of the 'Redefining the Electron' series. The electromagnetic compatibilities of electrons/positrons and photons are attributed to compatibilities between the toroidal and helical solenoid models.

The helical solenoidal form of a photon can be considered to be broken spin-torus, which is then stretched out in the torus's spin-axis direction and spinning to form a helical spiral. Its concentrated energy takes on a solenoidal pattern within a helical coil tube, and the helical coil itself rotates around its central axis which corresponds to its direction of movement (dashed red arrow in figure 1); the photon thus has small radius 'r' component, large radius 'R' component and lengthwise components to its movement. The helical solenoidal nature of photons is related to how they are generated, which shall be discussed shortly.

The helical form of the photon's concentrated energy has a solenoidal flow component is more compatible with the energy fields of electrons, positrons and CESs rather than their concentrated energy which has a purely circular flow within a closed torus. A photon has a wavelength ( $\lambda$  as shown in figure 1a); chirality; linear and circular momentum, albeit small; and its concentrated energy keeps moving forwards unless it collides with or is deflected by another object or particle. A beam of light consists of multiple p- and n-photons traveling in unison leading with their magnetic CO and AO poles respectively.

An electron (and a positron) has a rest mass of  $0.511 \text{ MeV}/c^2$ , but the rest mass of a photon is so small that it cannot be directly measured, although satellite measurements of planetary magnetic fields infer that it is in the order of  $3 \times 10^{-33} \text{ MeV}/c^2$ , and for practical purposes a photon is often considered to be massless. And as can be seen in figure 1b, in lateral cross-section, a photon is electrically neutral with a balance between the 3 AO-poles (A, C, E) and the 3 CI-poles (B, D, F). This explains why, unlike electron and positron emissions, light photons are not significantly deflected by large-scale strong magnetic fields acting even when acting perpendicular to their direction of travel. They may, however, be susceptible to small-scale electric field fluctuations such as surface plasmons: more about this later.

STEM contends that photons can be emitted by un-bonded out-facing CESs within the nucleons. Nucleons (figure 2) consist of three up/down quarks (U-D-U for protons and D-U-D for neutrons), and, as there are 6 CESs per quark, they consist of 18 CESs. However, CESs involved in inter-quark, offset or bitron bonding are unavailable for photon generation, but each nucleon would have at least 6 un-bonded CESs available.

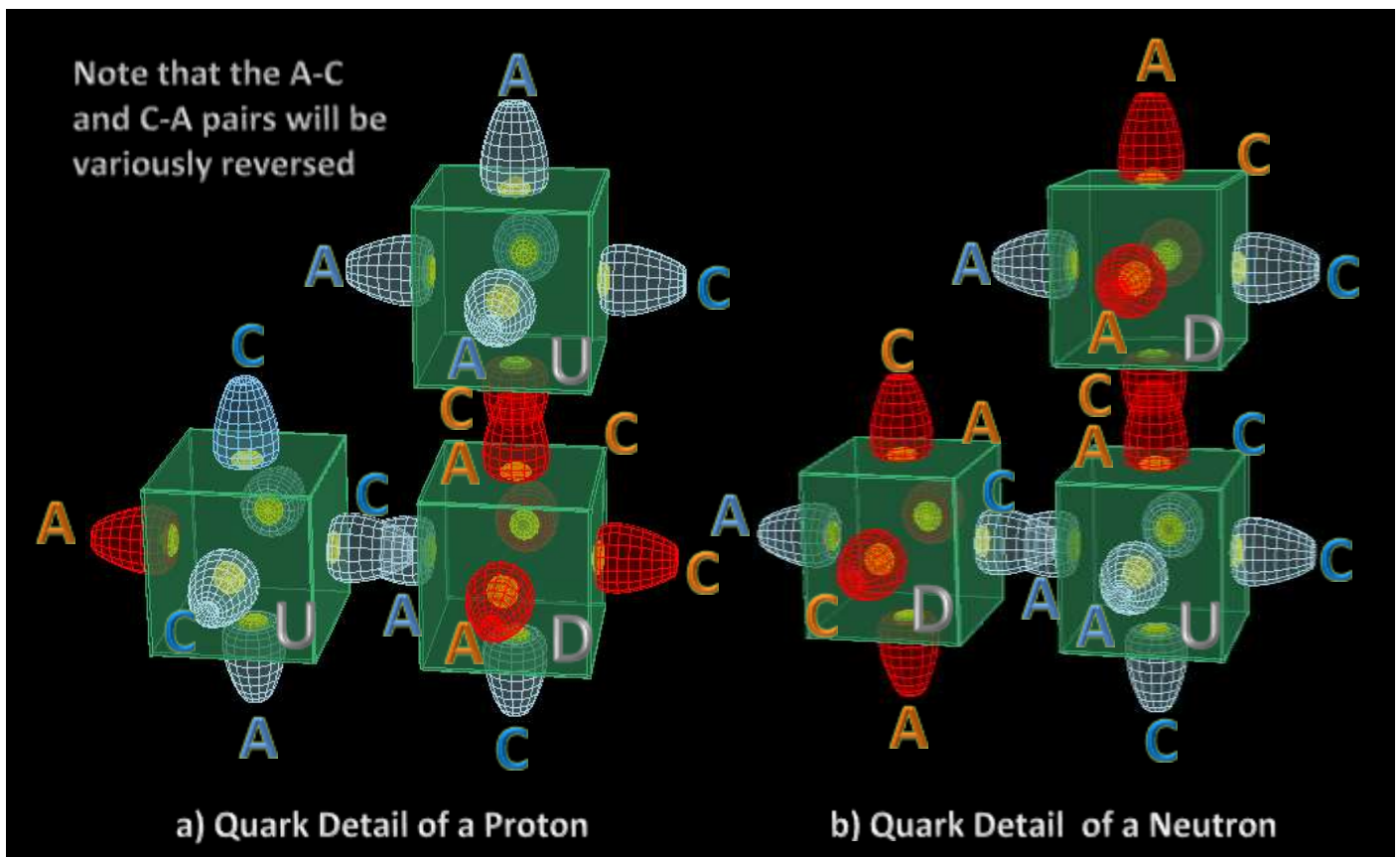


**Figure 2: Nucleon Quark Structure**

Within atoms, new photons can only be **created and emitted** as EMR by an out-facing AI or CI-pole CES. An energised environment builds up energy within quarks, and creates back pressure that causes energy congestion within the in-flow funnels of a CI/AI CESs so as to generate a **solenoidal torus** of concentrated energy (shown as a purple torus in figure 3a). As the congestion torus builds up within the in-flow funnel it expands outwards until, at a critical point, it is caught by the CES's out-flow field. This causes it to peel away spindle-like from its outer rim first into the spiral helical solenoidal form of a photon: its solenoidal form results from the swirling nature of the CES's outer energy field. The axial speed of ejection of the photon is the speed of the CES's out-flow energy, which we call the **speed of light**.

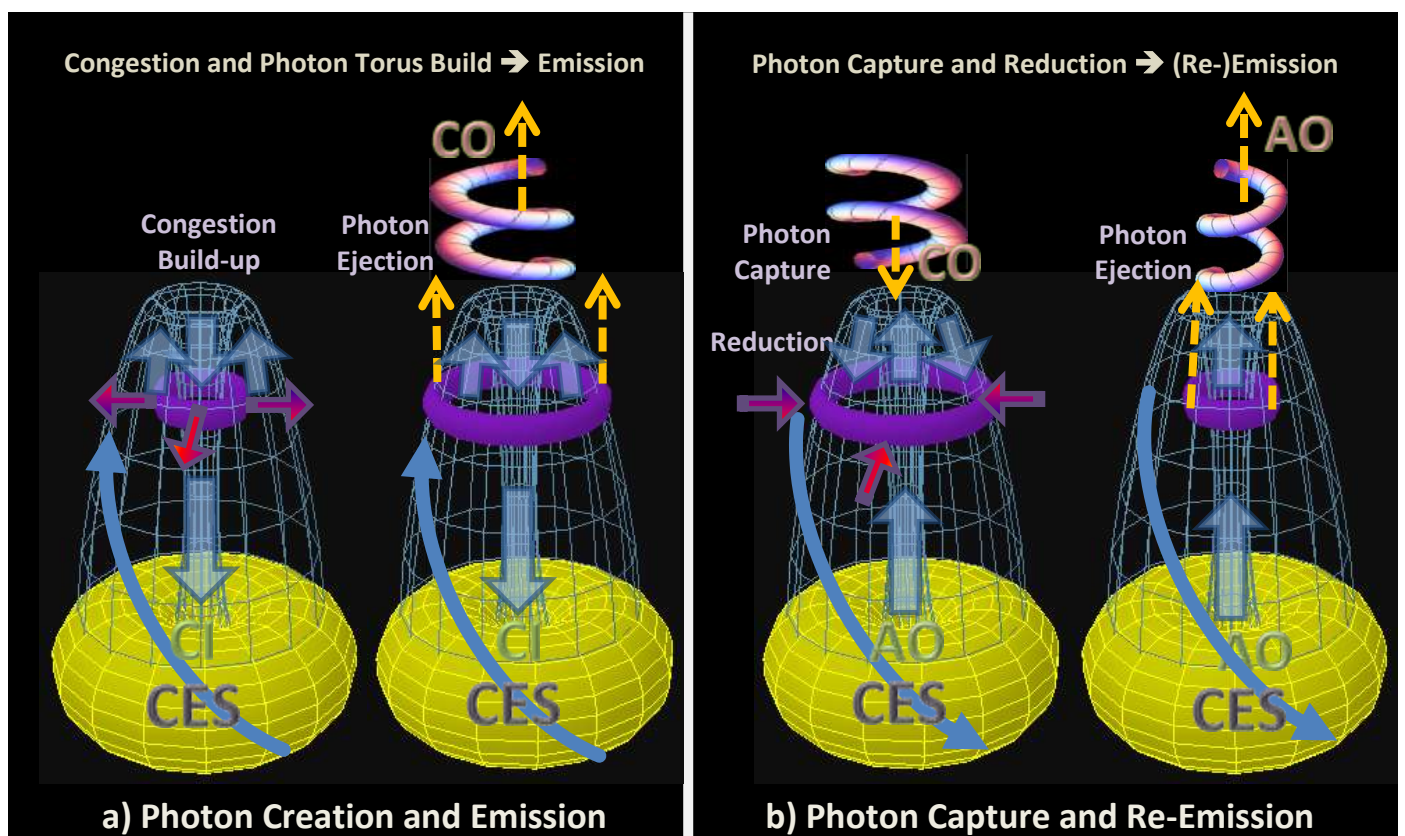


**Figure 3: Photon Creation/Emission and Capture/Re-Emission**

Photons can also be **captured and re-emitted** as EMR of a different wavelength by out-facing AO and CO-pole CESs (as shown in figure 3b). When a p-photon encounters an outwards-facing AO-pole CES, it can be captured by the CES's outer electromagnetic field with its helical form being concertinaed into a torus form (the larger purple torus). The captured photon can be temporarily held in limbo before being released as a photon of approximately the same energy level and frequency, but with **reverse helicity**. This involves minimal energy transfer between EMR and matter.

However, particularly in a highly energised environment, energy exchange between captured photons and atoms is more likely than the temporary hold-and-release scenario. For the energy exchange scenario, the captured photon starts to lose energy to the CES's outer energy field, thus reducing its large radius size. The shrinkage of the torus's large radius continues until it is completely consumed by the CES (total absorption), or until it is picked up by the CES's central out-flow vortex funnel and ejected. The ejection process causes the now shrunken torus to peel away spiral-like from its inner edge, exiting with the helical solenoidal form of a photon. Its solenoidal form results from the swirling nature of the CES's central out-flow field. The photon so created has reverse helicity (or chirality) to the captured photon, and leaves with reduced energy and frequency (and commensurately increased wavelength).

Similarly when an e-photon encounters an outwards-facing CO-pole CES, it can also be captured and released with the reverse helicity as a p-photon with reduced energy and frequency.

The frequency of the helical solenoid form of a photon is proportional to  $R/(r.N)$ . Assuming that the number of turns per unit length ( $N$ ) and the small radius ( $r$ ) of the captured and re-emitted photons are approximately the same, then the reduced large radius ( $R$ ) means that the frequency, and thus the energy, of the re-emitted photons is reduced and wavelength increased. The increased effective wavelength is analogous to the **Compton Effect**, wherein the wavelength of X-rays and other energetic electromagnetic radiation is increased by the elastic scattering.

The emission spectra of elements and compounds provide excellent examples of the photon creation and capture/re-emission processes. Each element in the Periodic Table is capable of creating and emitting EMR with one or more wavelengths which are dictated to geometry of their atomic structure as well as the availability and location of unbonded out-facing CI-pole and AI-pole CESs. These photons are collectively referred to as the **base EMR**.

Similarly each atom type can only capture photons of particular wavelengths, as dictated by the availability of unbonded out-facing CO and AO-pole CESs, and re-emit them as lower-energy photons of increased wavelength with reverse chirality. These photons are collectively referred to as **rebound EMR**. The combination of base and rebound EMR create the multiple bands of specific wavelength combinations that present as emission spectrum that are

unique for each element, examples of which are shown in figure 4, with the weaker rightmost colour bands being more representative of rebound EMR.

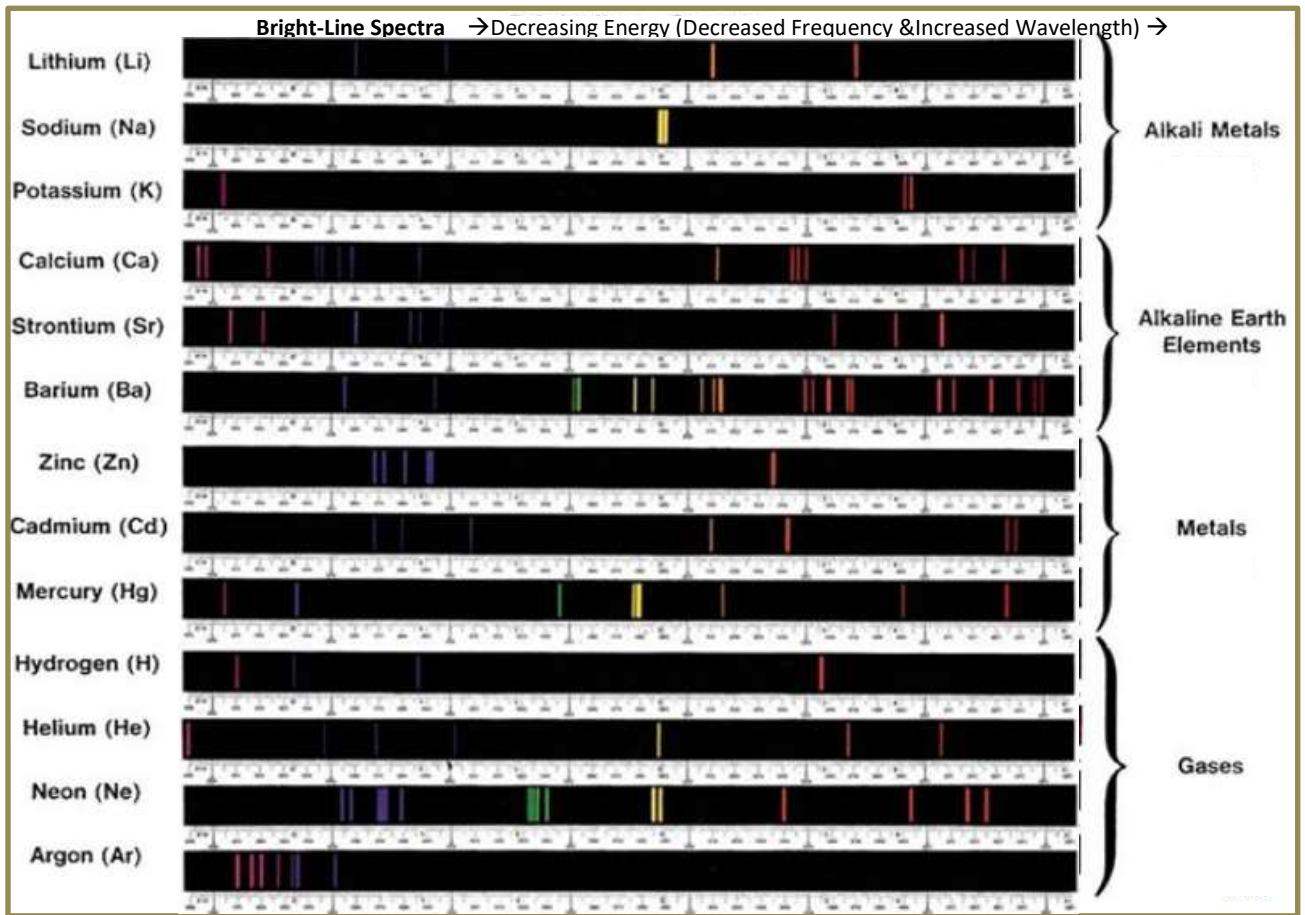


**Figure 4: Emission Spectra for Common Element Groupings**

Base and re-bounce frequencies are related to the orientation of out-facing un-bonded CESs, and their field strength which is mainly dictated by the **energy capacitance** of nucleon layers within the atom. The energy capacitance of nucleon layering is related to its geometric shape (which dictates layer size), the number of the connected layers and the nature of the connectivity (i.e. inter-quark and bitron connections). The geometry of each layer and its inter-connectedness with other layers results in the unique range of quantum-like base and re-bounce frequencies of elements and related compounds.

For many elements, base and rebound photons can be re-captured and re-emitted several times, producing increased numbers of re-bounce bands, with most re-capture occurring between neighbouring atoms but also possibly internally within the polygonal nucleon layers themselves.

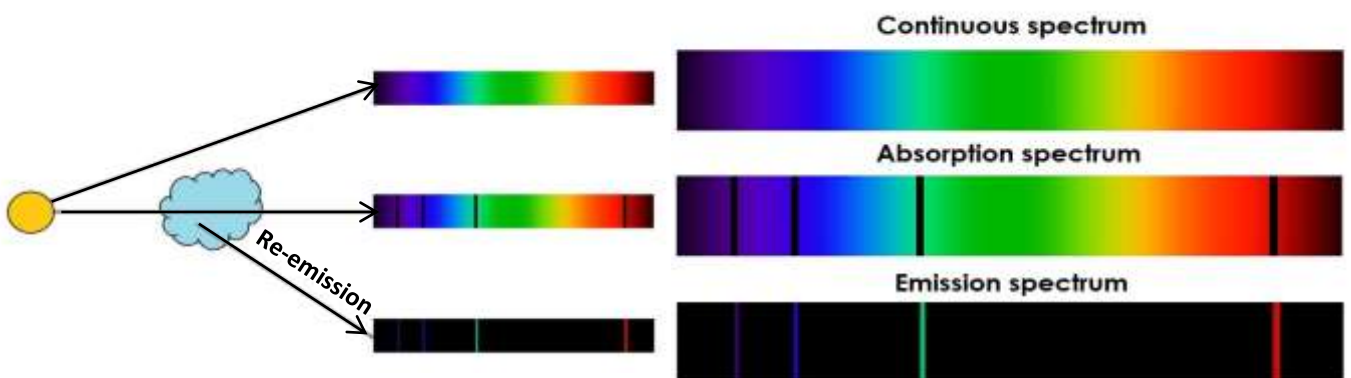


**Figure 5: Absorption and Re-Emission Spectra**

A spectacular example of the hold-and-release scenario is **spectral line absorption**, wherein photons with the optimum quantum frequencies are captured from incident light and held by the material involved. This produces dark bands in the absorption spectrum corresponding to the captured photon frequencies. The captured photons can in turn be released with energy levels and frequencies very close to their pre-capture state, appearing as solitary bands in the material's emission spectrum, as demonstrated by gaseous cloud example as represented in figure 5.

EMR represents a major way in which energy (radiant) is transferred between bodies. Some photons from incident EMR are electromagnetically repelled (reflected) or diverted (refracted); others become attached to or absorbed by nucleons. Bodies gain energy by capturing photons and partially (or fully) absorbing photon energy and releasing lower energy re-bound photons. The extra energy acquired feeds back into the atom's nuclear nucleon layers, adding to the net energy level of the atoms involved. When in an excited state, atoms create and release energy as EMR to reduce their net energy level. In balanced environments atoms are more likely to hold-and-release photons with very little energy exchange between the two.

A **beam of light** is Electromagnetic Radiation (EMR) within the visible light frequency range consisting of a mixture of p- and e-chirality photons and a range of frequencies. In a similar fashion to how electrons and positrons form strands within an electrical conductor, p-photons have a propensity to align and keep in line when they are end-on-end adjacent, and similarly for e-photons. Thus photons become marshalled into linear strand-like p and e-photon groups, but unlike electrons and positrons forming an electric current, they all move in the same direction as a beam of light.

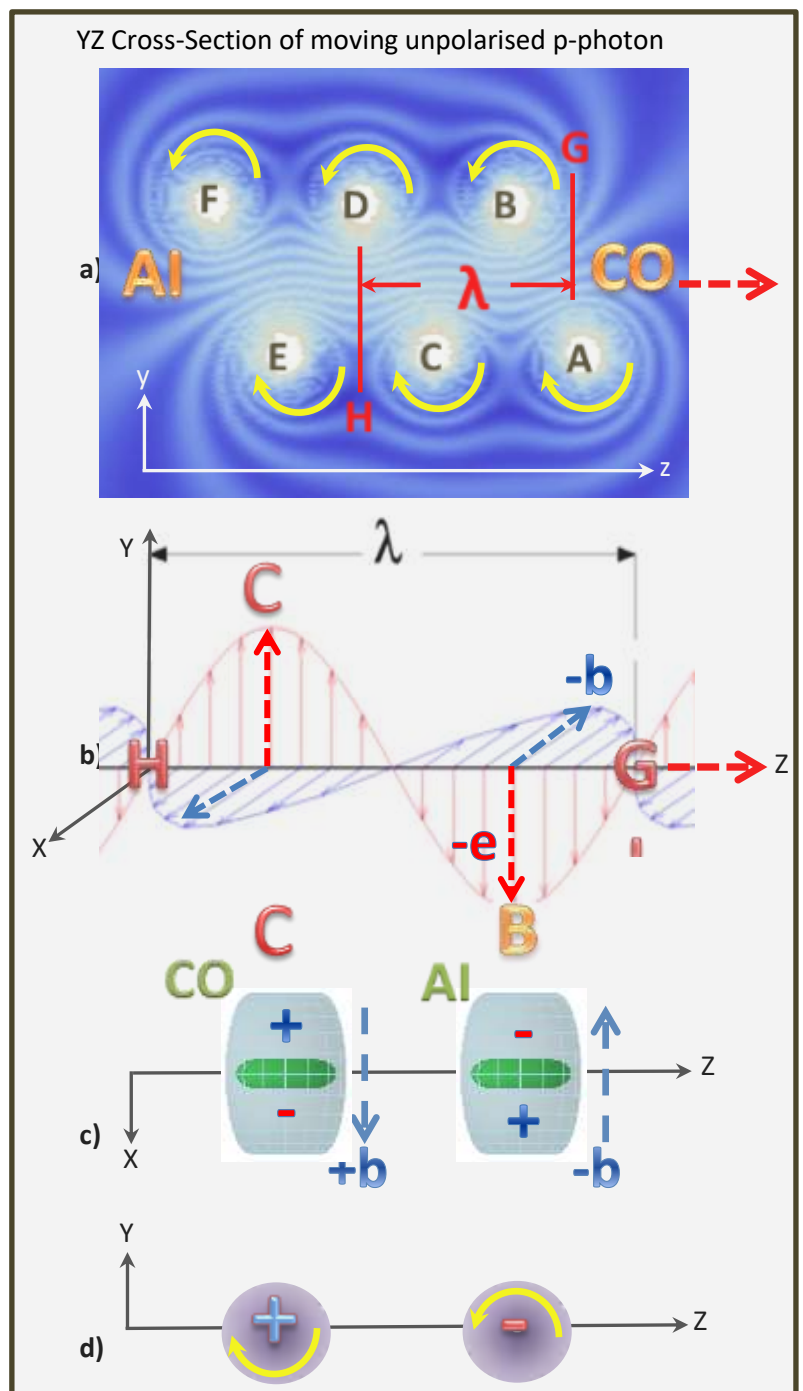
Thus, although individual photons in the visible light range represent very small concentrations of energy compared with electrons, positrons and CESs, the strand-like grouping results in a light beam that is more robust and stable than could be expected from a random group of independent photons that would most likely interfere with each other.

Figure 6 shows how the in-phase sinusoidal electric and magnetic fields associated with unpolarised light are generated. Referring to the YZ-plane cross-section of the unpolarised p-photon moving down the Z Axis (6a), the first electrical maximum after point G passes by is at point B of the photon helix.

Looking from the +Y axis onto the XZ plane as in 6c, point B presents as a small disc-like piece of the photon's concentrated energy (the green disc that is reminiscent of the side profile of an electron torus). The disc's magnetic field (-b) is parallel with the X axis and is thus perpendicular to the negative electric field in the YZ plane (6a). As the implicit electric field is AI negative (-e) in the YZ plane (6d), the point B field components plot as values -b and -e in 6b.

The next electrical maximum in the YZ plane after point B is point C, which has a positive CO implicit electric field (+e), and, because the electromagnetic energy is moving in the opposite direction to that at Point B, the magnetic field direction is reversed (+b), as shown in 6b. The electrical and magnetic fields reduce in sinusoid fashion from B to C with zero values at points G and H (and to the mid-point between B and C) to complete one complete sinusoidal cycle represented by wavelength  $\lambda$  in 6b.

Photons can be packed together with their helical spirals entwined to form **Optical Vortex Light** as in figure 7a. Optic vortex light is associated with **Orbital Angular Momentum (OAM)**, which is sufficient to rotate and manipulate nanoparticles (figure 7b). The electromagnetic fields of the off-set and entwined helical photons interfere with each other to generate circular zones of interference when viewed end-on (leftmost in figure 7a).



**Figure 6: Unpolarised Photon Electromagnetic Fields**

Optic vortex light can be produced by a range of techniques including Spiral Phase Plates (SPP), Q-plates, pitch-fork holograms and cylindrical mode converters.

To entwine the photons must have the same chirality, which dictates the left- or right-handedness of the optic vortex light, with the ' $\ell$ ' factor (7a) indicating the number of photons helically entwined to form each composite photon.

More common and less exotic than optical vortex light is **polarised light**. The helical solenoidal structure of photons is quite fragile, and can easily be modified by transmission through polarising materials: these mechanically convert its circular cross-sectional profile into the elliptical profile of partly polarised light, or completely flatten into the sinusoidal lengthwise profile of planar polarised light. Alternatively the helical coil can be uncoiled and flattened mechanically by the process of reflection by a polished non-metallic surface (e.g. glass) to form plane polarised light.

Considering reflection option (7d), as the leading head of an unpolarised photon reaches the reflecting surface the helical solenoid tube of concentrated energy is simply uncoiled to take on a planar sinusoidal transmission form which is called **Planar (or linear) Polarised Light (PPL)**, and oscillates in a plane perpendicular to the I-R plane (the plane containing the incident and reflected light paths). PPL thus generates a sinusoidal electric field perpendicular to the I-R plane and a magnetic field perpendicular to and in phase with the electric field, forming a pattern similar to that for unpolarised photons, albeit a somewhat attenuated one. Thus, although unpolarised and polarised photons have different energy forms (helical and sinusoidal respectively), their electromagnetic footprints are quite similar.

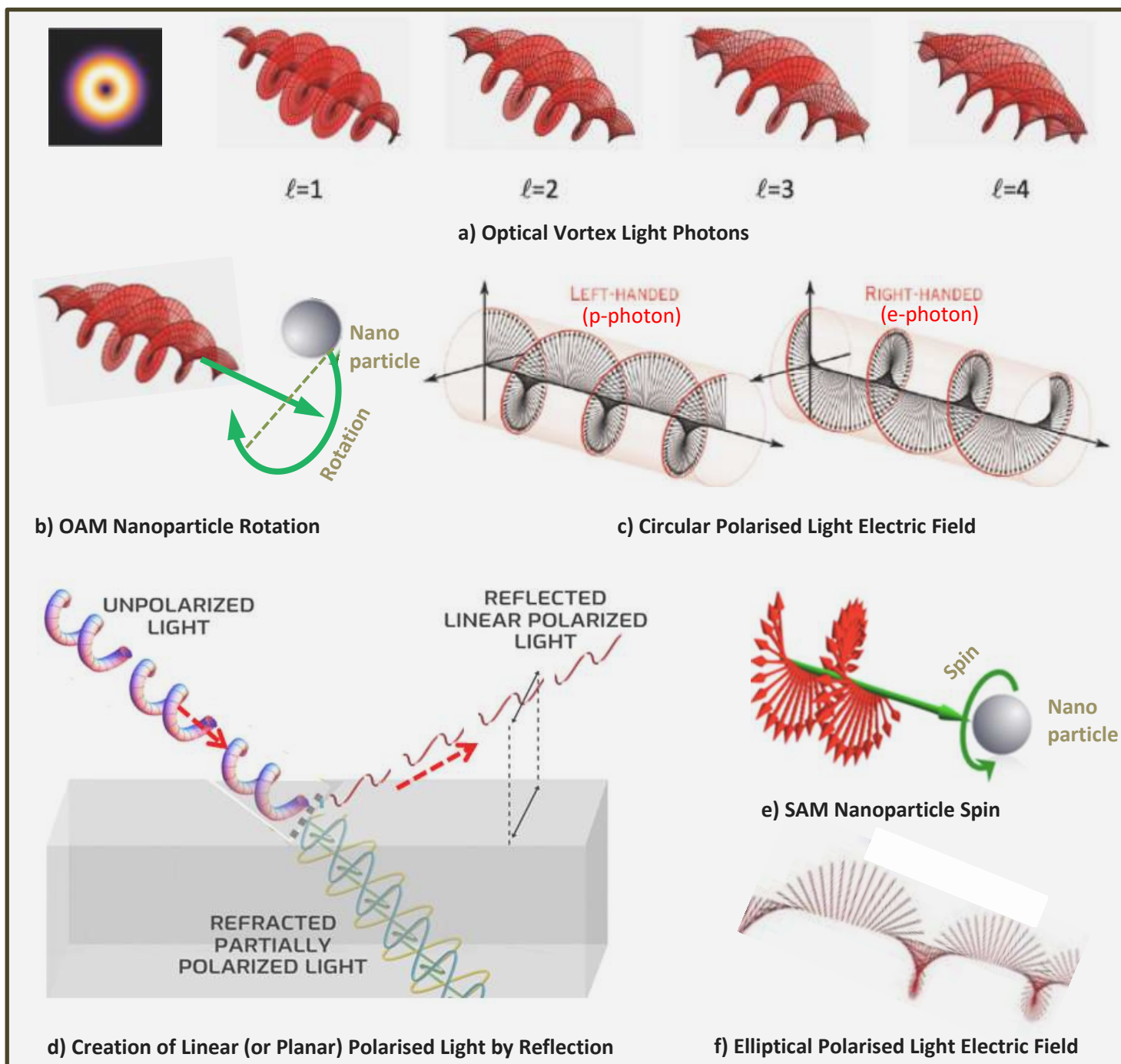


**Figure 7: Optic Vortex and Linear, Circular and Polarised Light Forms**

**Circular polarised light** occurs when photon groupings whose polarisation planes are perpendicular to each other, having equal amplitude and a phase difference of  $\pi/2$ , are combined. This creates light with an electric field that rotates in a circle around the direction of propagation, with a left- or right-hand rotation effect (7c) resulting from the chirality of the component photons. Circular Polarised Light is associated with **Spin Angular Momentum (SAM)**, which, while not being as strong as the OAM of optical vortex light, is sufficient to cause nanoparticles to spin (7e).

As for unpolarised light, when a circular polarized light beam is reflected by a conventional (or regular) mirror, the mirror reverses the beam's spin state, so that the light it reflects back out has the **opposite** spin or chirality as the incident light (figure 8a). A **chiral meta-mirror**, on the other hand, reflects circular polarized light with the same spin of the incident beam, but only for one spin state, with a beam with the opposite spin being completely absorbed. Chiral meta-mirrors are available to reflect either right (8b) or left (8c) circularly polarized light, and do so without a change of chirality; but each can only reflect light of 1 chirality, with light having the opposite chirality being absorbed.

**Elliptical polarised light** (7f) is a more asymmetrical form of circular polarised light with the combination of 2 perpendicular linear polarised light components with differing amplitudes and a phase difference of  $\pi/2$ .

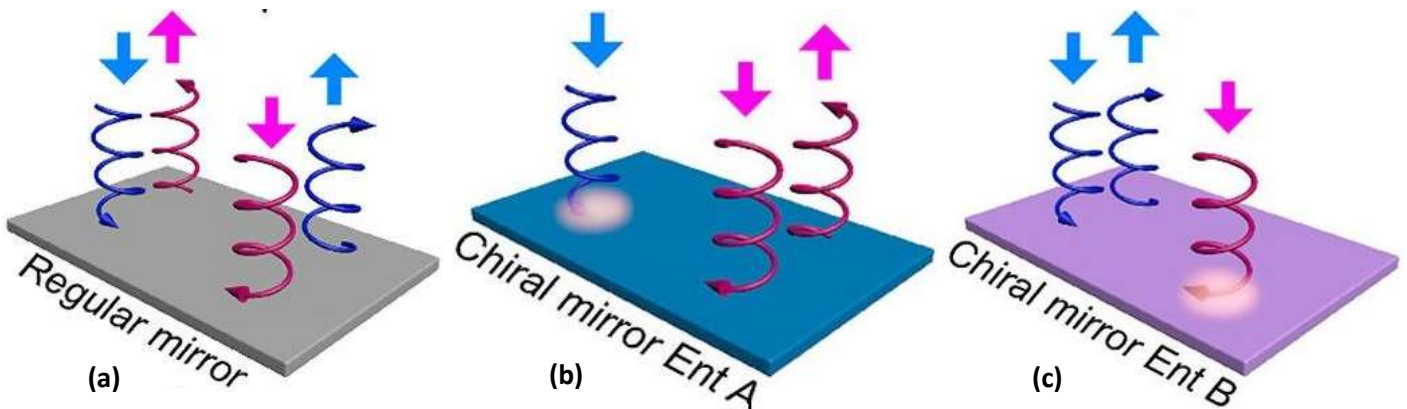


**Figure 8: Reflection of Circular Polarised Light**

## Light Refraction

Light **refraction** occurs when light passes from one medium into another that has a different **refractive index**. When light passes from a fast medium (e.g. air with  $n=1.0$ ) to a slow medium (e.g.  $n=2.0$  as in figure 9), the denser medium axially compresses the photons, thus reducing their wavelength and linear forward speed.

The net result is that their frequency remains unchanged, as can be seen in figure 9. When the helical coil of the photons is compressed so, its overall length (if straightened out) remains unchanged, and the speed of the energy flow within the helical coil remains the same. However the circular-to-linear (linear being the direction of photon travel) flow ratio has increased: thus the energy spends more time travelling in spiral circles which results in reduced wavelength and net linear speed.

The reverse takes place when the photons pass into a medium with a lower index of refraction, with their wavelength and forward speed increasing as their helical coil form stretches.

For 'white' light containing multiple photons with a range of different wavelengths, proportional refraction causes a rainbow-like separation of the light components, as for the glass prism shown in figure 9.

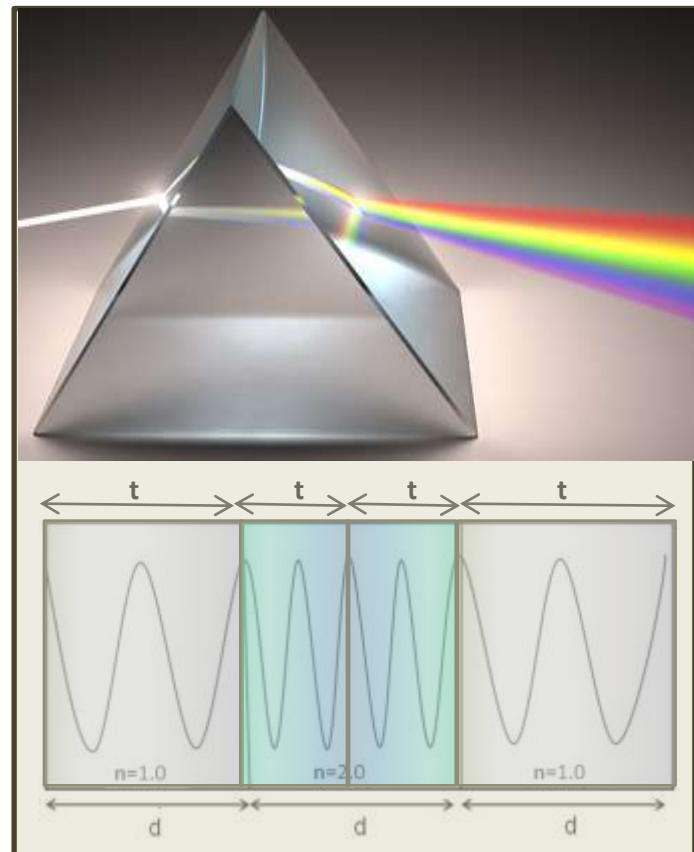


**Figure 9: Light Refraction**

# Constructive and Destructive Interference

Constructive and destructive interference of intersecting standing wavefronts is well understood and documented. However, experiments involving the constructive and destructive interference of light and its extension to electrons, nucleons and molecules, needs to be considered and explained in terms of the STEM approach.

Starting point is consideration of the interference patterns derived from a **Michelson Interferometer** setup for parallel merged beams as shown in figure 10. A single beam of **coherent light** (i.e. light whose photons have the same frequency and a constant phase difference) is split into two identical beams by a partially reflecting mirror beam splitter. Each of the split beams travels a different path to be re-combined before arriving at a detector. The path length difference of each beam creates a phase difference between them, producing a characteristic concentric interference pattern (such as that in figure 11a).

At the beam-splitting mirror M, approximately half the light is reflected as linear polarised light heading towards reflecting mirror M1, where it is reflected towards the detector E. The rest of the split beam from M strikes reflecting mirror M2 and sent to the reverse side of mirror M ( $C^1$ ) where it is linear polarised and reflected towards the detector E. The interference patterns formed (figure 47a) are circular because the virtual images  $S_1'$  and  $S_2'$  of the light source form with one behind the other, and photons further from the centre of the beam travel fractionally further distances causing the interfere to vary radially.

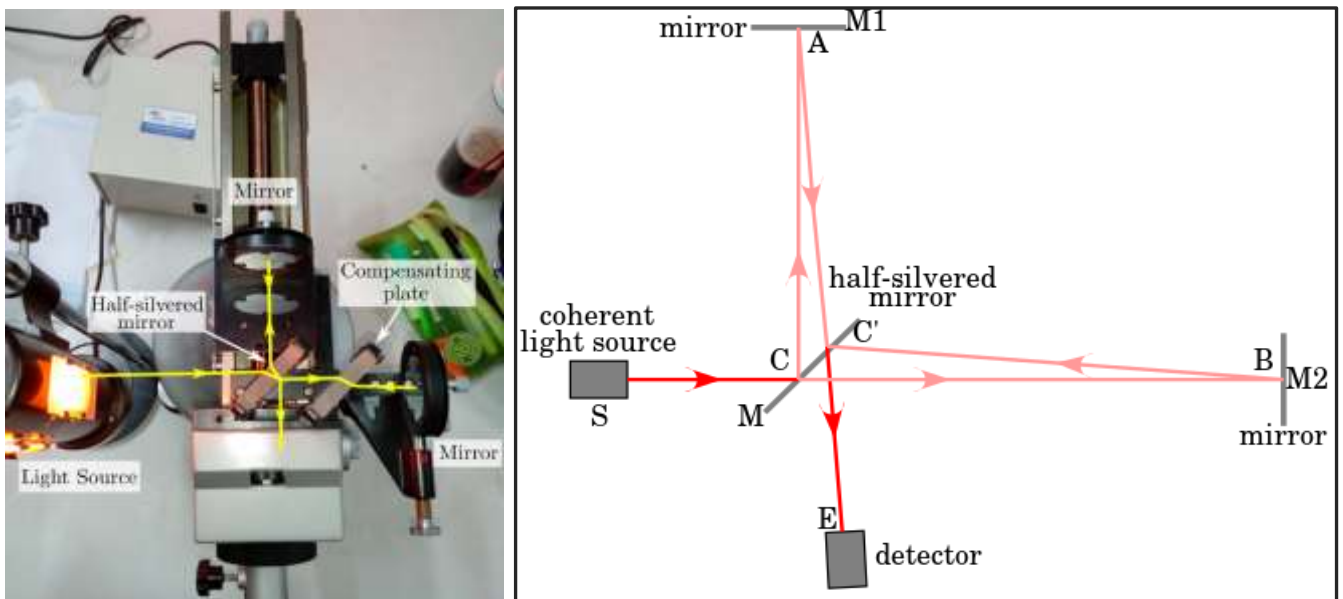


**Figure 10: Michelson Interferometer setup: parallel merged beams**

For the inclined Michelson Interferometer setup, a slight angle between the two returning beams caused by the inclined mirrors M1 and M2 results in a sinusoidal fringe pattern as in Figure 11b. If there is perfect spatial alignment between the returning beams, then there will not be any such pattern but rather a constant intensity over the beam dependent on the differential path length.

For the inclined Michelson Interferometer the interference patterns are formed by the side-by-side virtual image ( $S_1'$  and  $S_2'$ ) offset.

When linearly polarised STEM-style photons with the same frequency are superimposed upon each other, as with the Michelson Interferometer, standing wave interference takes place, creating the interference patterns observed.

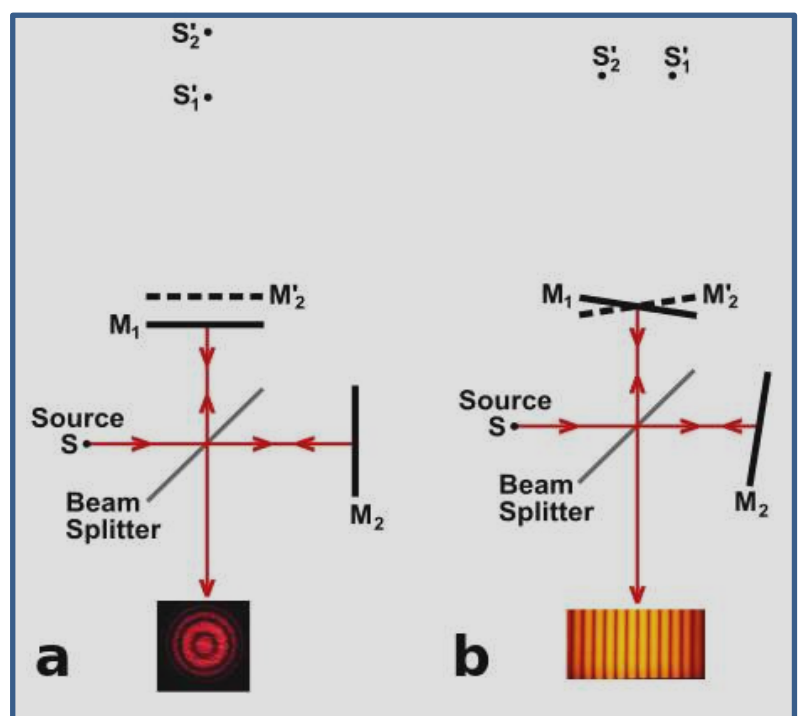


**Figure 11: Michelson Interferometer Interference Patterns**

Whereas the way in which photons are polarised and superimposed by the Michelson Interferometer are easy to explain, an explanation of the interference patterns for the 2-slit light and electron experiments is less obvious.

**LSPRs (Localized Surface Plasmon Resonances)** are collective electrical oscillations in metallic nanoparticles, especially gold, that are excited by light, and which exhibit light scattering peaks and strong electromagnetic near-field enhancement. LSPR field are highly localized and decays away from the gold/air interface. A very important aspect of LSPRs is their light-intensity enhancement and localization means the LSPR has very high spatial resolution, and effects such as the magneto-optical effect (the Faraday Effect) are enhanced by LSPRs.

**SPPs (Surface plasmon polaritons)** are visible-frequency electromagnetic waves that travel along a metal–dielectric (e.g. metal–air) interface. SPPs involve charge motion in the metal (the surface plasmons) and electromagnetic waves in the air (the polariton aspect). SPPs are thus a type of surface wave, and are shorter in wavelength than incident light photons. Some SPP energy is lost to absorption in the metal with the rest scattering into free space. And **importantly**, when a SPP wave interacts with an irregularity, such as a surface corner or edge, **part of the energy can be re-emitted as light**.

Figures 12a and 12b are visualisations of surface plasmon electric fields; 12c is an emission profile at  $\lambda = 580$  nm of a micro-hole lens using FDTD simulation from the 2014 paper by [S. Saxena et al on Plasmonic Micro Lens](#) and 12d, a depth of focus plot (pink area) for wavelength ranging from 400 nm to 700 nm from the same paper. The micro-hole lens uses both the phenomenon of diffraction as well as surface plasmons to focus the incident light. It exploits the principle of superposition of the incident planar wavefronts and the diffracted non-planar wavefronts coupled to surface plasmon waves to generate high energy concentration at the focal spot. This technology demonstrates the ability of SPPs to diffract (i.e. bend) and manipulate light and is thus relevant to the double-slit experiment.

The diffractive effect of SPPs as photons pass through the slits (possibly related to electro-optic effects such as the [Kerr Electro-Optic Effect](#)), the electromagnetic drag on photons moving close to the sides of the slits; and **far-field scattering** all are factors that contribute to the creation of curved wavefronts (figure 13) for light passing through narrow slits lined with gold film. STEM contends that such curved wavefronts (figure 13a) radiating from each slit creates interference bands such as those of shown in figure 13b.

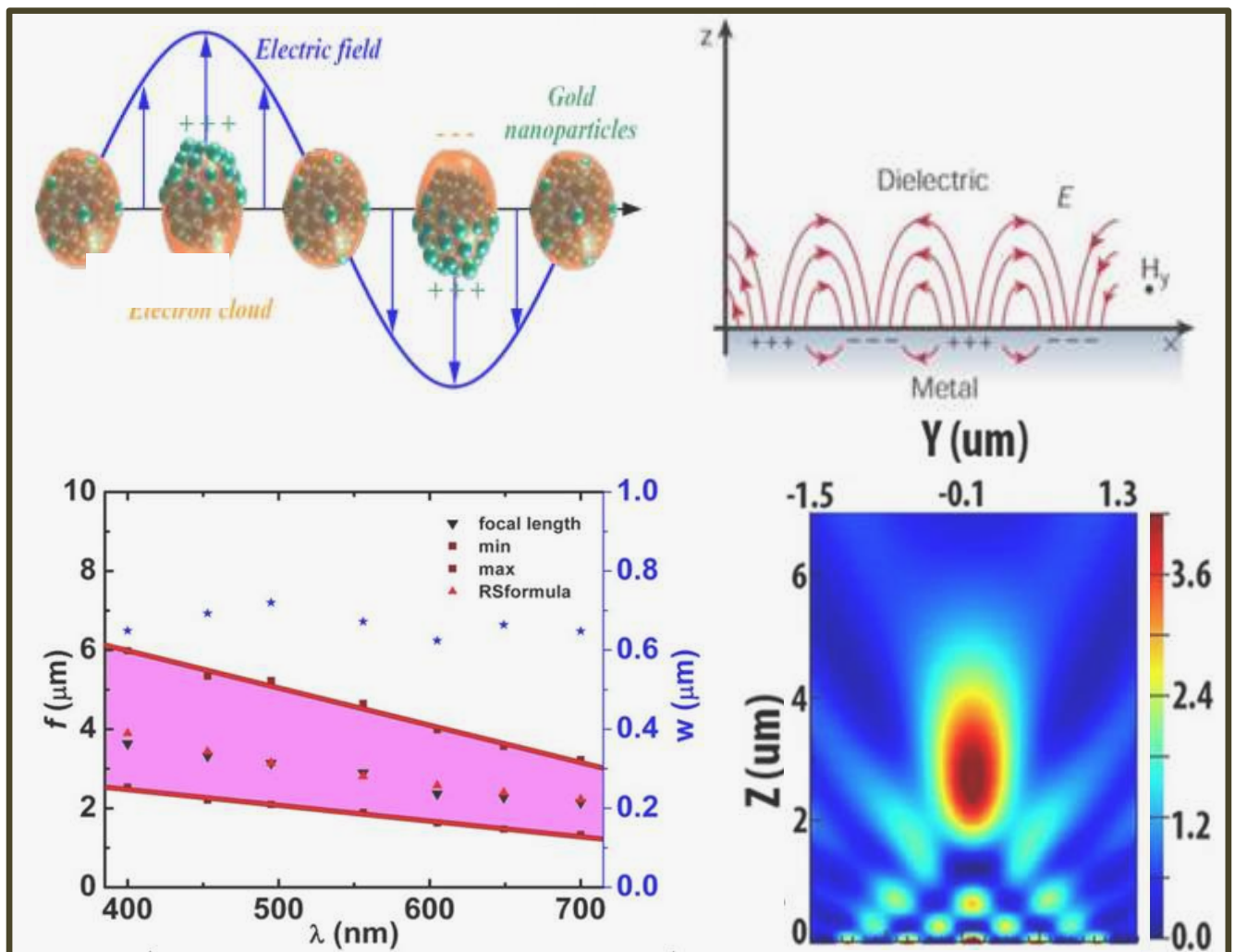


Figure 12: Surface Plasmons and Far-Field Scatter Effects

Michael Mishchenko's 2006 paper '[Far-field Approximation in Electromagnetic Scattering](#)' indicates that far-field patterns are geometrically generated, which would mean that of curved wavefronts can be created even without the effect of SPP refraction: whilst considered to be a factor STEM remains unconvinced that geometry alone is sufficient.

SSPs were discovered in the 1960s, with well-established research available since 1970 and their widespread use for surface plasmon resonance spectroscopy and related Nano-technologies. Thus it is rather strange that the double-slit experiments have not been re-visited and re-interpreted taking into account the possible effects of far-field geometry and SPPs.

Instead the double and single slit experiments have been modified to include electrons and atoms as Quantum Mechanics seeks to extend wave-particle duality to all matter.

An example of the single and 2-slit experiments involving electrons is the 2013 paper titled '[Controlled double-slit electron diffraction](#)', by Roger Bach et al. This paper provides an excellent historical overview of the most significant experimental evidence on the subject since Richard Feynman's thought experiment concept. It is one of the few papers to provide full details (although the backstop distance is missing) of the setup for continual electron and single electron-by-electron accumulation, together with good clear presentation of the results.

The wall and mask (bottom right of figure 14) were constructed from 100 nm thin silicon-nitride membrane coated with approximately 2 nm of gold (which is an ideal medium for SSP generation), and the slits are 62nm wide and separated by 272nm.

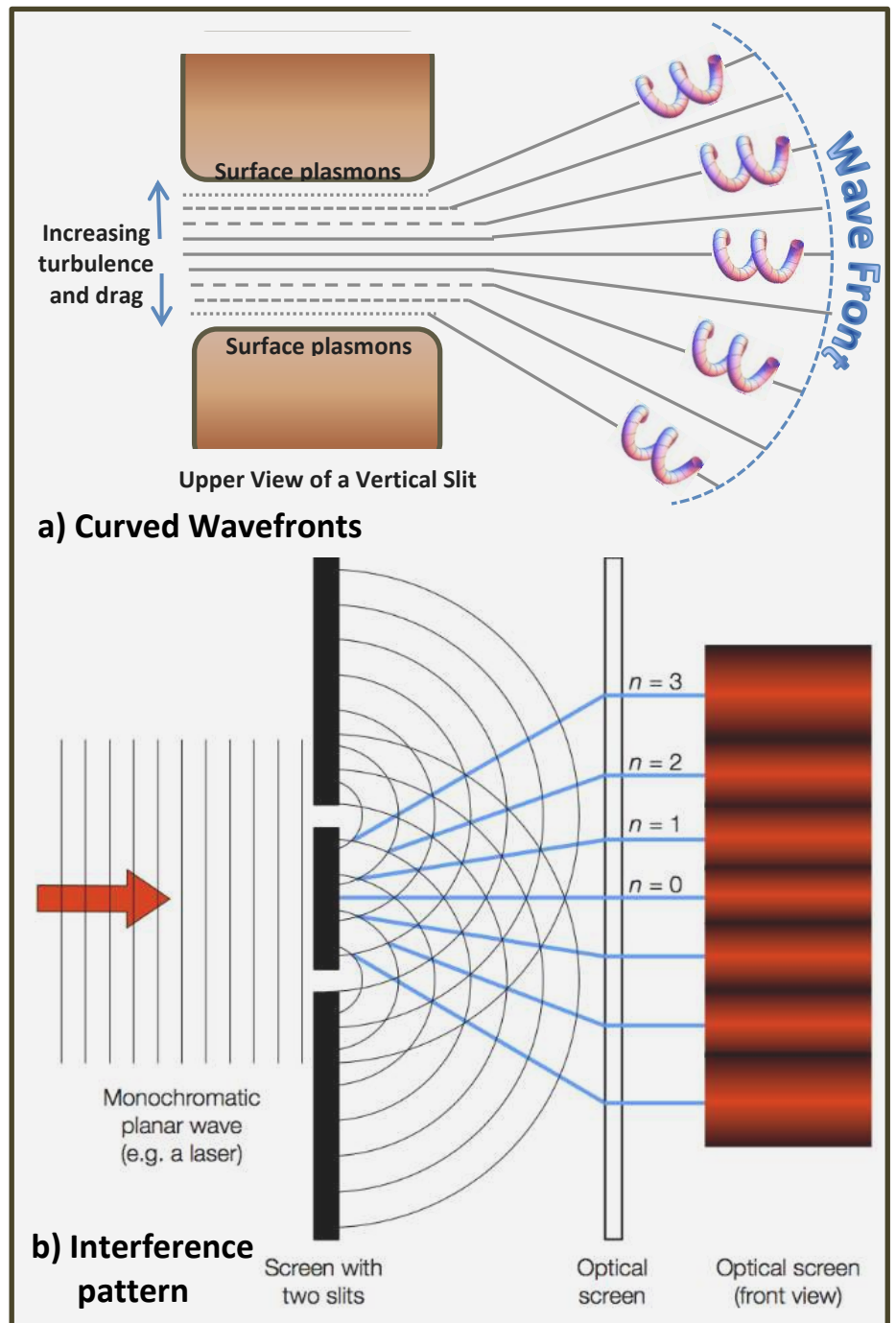


**Figure 13: 2-Slit Experiment for Light**

STEM contends that a combination of light and electrons passing through the narrow slots generate SSPs that cause a scattering of the electrons, forming a curved wavefront pattern analogous to the far-field scattering for light. Such curved wavefront patterns, which would in turn produce a series of overlapping skewed distributions of electrons striking the backstop as shown in figure 14, wherein the electron contribution from each slit is shown in blue for the upper slit and red for the other. The net distribution of electron hits is shown by the dashed green line plot: it corresponds well to the banded pattern  $P_{12}$  to the right of figure 13, and is not dissimilar to that of figure 13b.

The banded pattern  $P_{12}$  of figure 14 is an intensity enhanced version of the electron distribution at the backstop. With progressive plots for single electrons there is no chance that electrons might interfere with each other because although their paths may cross, they are never in the same place at a given point in time. However, using the 6235 single electron distribution as shown bottom left in figure 14, by projecting the hit points to a central axis and then represent the projected plot as an intensity enhanced plot, the result are almost identical to that of  $P_{12}$ , and without any possibility of constructive and destructive interference being a factor.

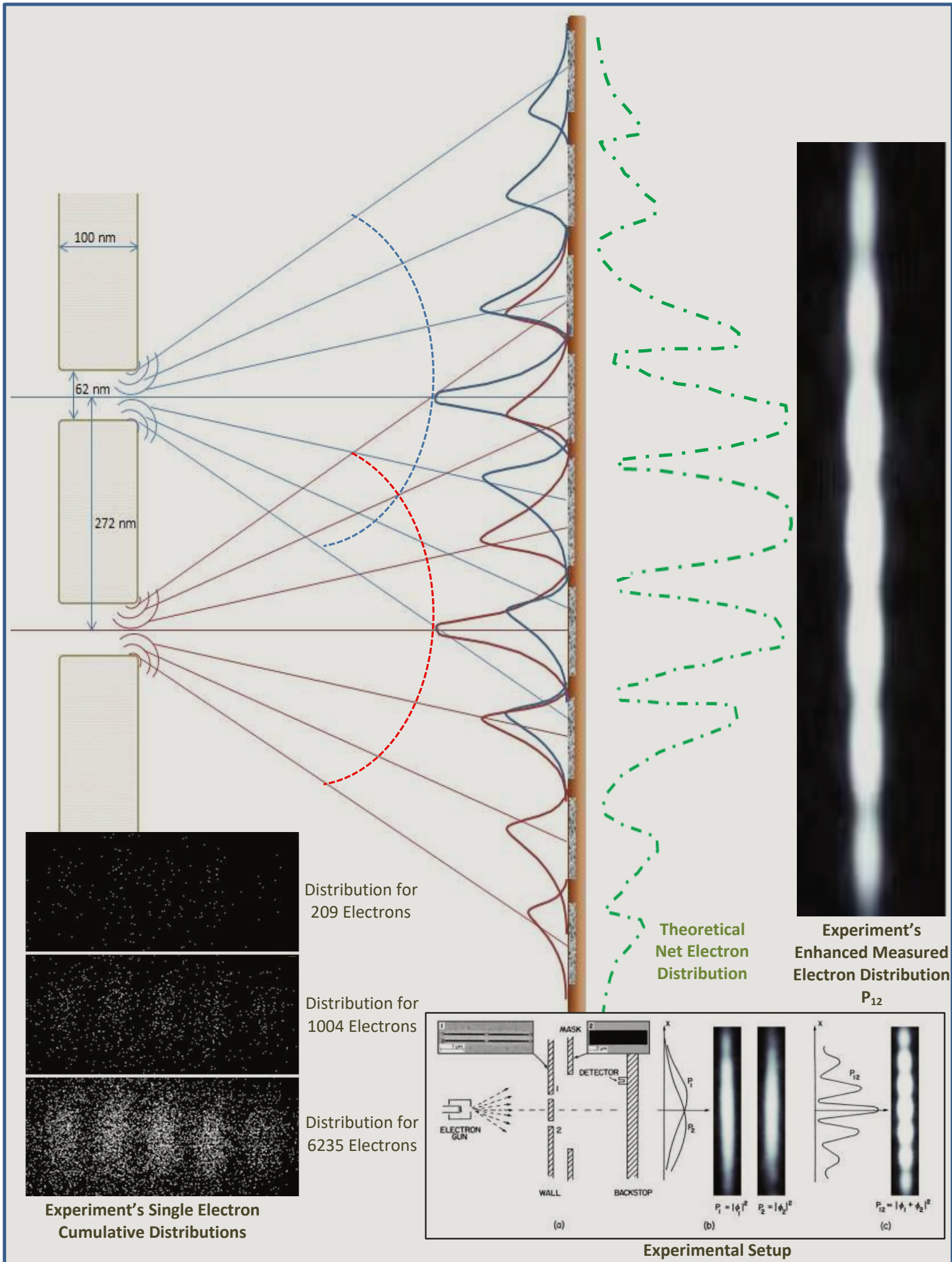


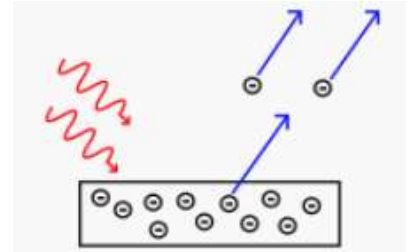
**Figure 14: 2-Slit Electron Electromagnetic Deflection and Distribution Pattern**

For the continuous streaming of electrons (as opposed to the single electron firings), It is probable that some electron pairs will deflect each other should their paths cross, but such deflection, and related electrical interference between the pair, is far removed from them destructively eliminating each other.

For light the 2-slit experiment is easily duplicated, with the banding being explained by the constructive and destructive interference of intersecting curved wavefronts of light. The story for 2-slit experiments using electrons, atoms and molecules is different: the patterns observed here represent a statistical distribution of deflected particles on the target screen or sensors. It is the author's opinion that the 2-slit experiments do not demonstrate, confirm or bestow particle-wave duality characteristics to electrons, atoms, molecules or, by logical extension, to matter, even though such wave-like characteristics can be accommodated by Dirac's wave equations. Protagonists of this approach would do well to understand that a satisfied theory equation does not equate to a satisfying practical explanation.

## The Photoelectric Effect

Photons arriving at the surface of an incident medium can be variously scattered; or cause the emission of photo-electrons; or cause electron-positron pair production: it is the energy level and incident angle of the photon that are the main factors influencing the outcome.



Scattering can be **coherent scattering**, which is simple deflection that is analogous to reflection, or it can be **Compton scattering** that causes the emission of an electron and a photon of wavelength greater than the incident photon, and is called the **Compton Effect**.

When only an electron is produced it is called a **photo-electron** and the process called the **photoelectric effect**. It represents just one of the 4 possible outcomes as outlined above.

**Pair production** is when an electron and a positron are produced.

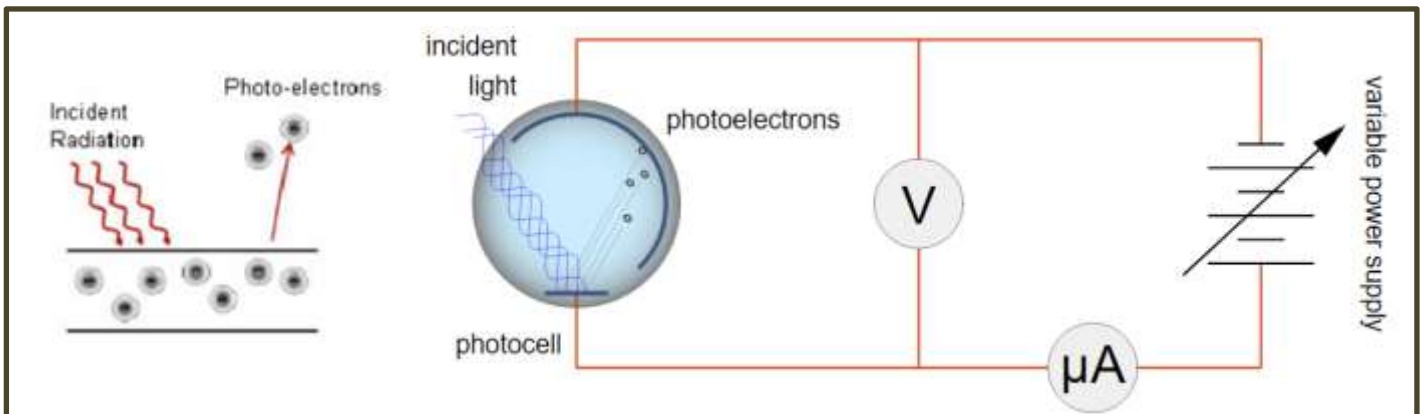


**Figure 15: The Photoelectric Effect**

Figure 15 represents a simple form of solar photocell that incorporates a stopping-current setup that is typical of those used for photoelectric demonstrations. More elaborate [experimental setups](#) involve light filters to control the wavelength of the incident light.

Incident photons that have a frequency above the **threshold frequency** of the incident medium's surface layers, can collide with an atom and release a bitron as a free positron or electron. Although positrons and electrons are released in approximately equal numbers, only electrons are emitted. This is because free positrons, moving their CO-pole leading, are held back by the net pull-force of the outer proton layer of host material (a pull analogous to the pull of an offset bond) and need significantly more kinetic energy than an electron to break free from the host medium. Electrons, on the other hand, because they have a reverse spin to the proton layer field receive an extra push away from the host material. Positrons require more than double the kinetic energy to escape the host material than that required by electrons and hence no positrons gain sufficient kinetic energy from the photoelectric effect regardless of the directness of the photon hit.

Emissions from medium to low energy processes (e.g. electron guns and the Photoelectric and Compton Effects) consist of entirely of electrons. A high energy particle accelerator, such as described in Part 1, is needed to provide positrons with sufficient energy to escape their host material as free positrons.

Only electrons created by direct photon-hits can acquire sufficient momentum to escape the incident medium. Those electrons created by oblique or glancing bitron blows either gain insufficient momentum to escape the surface or insufficient kinetic energy to reach the receiving plate should they escape. Positrons have no such chance.

The inability of positrons to escape results in an increase in the positron-to-electron ratio within the incident medium, which, referring to figure 15, with the accumulation of captured electrons at the receiving plate, creates an emf aligns the electrons and positrons. This causes electrons to start shuffling from the receiving plate (electron source) towards the incident plate (electron sink); and the synchronous movement of positrons from the incident plate (positron source) towards the receiving plate (positron sink).

By applying an opposing emf, electron build-up increases at the receiving plate which, at the **stopping voltage**, can prevent even the most kinetically energetic of the ejected electrons from reaching it. This allows the maximum kinetic energy of the emitted electrons for a given EMR frequency to be determined. Such measurements confirm a linear relationship between kinetic energy and photon frequency that varies depending upon the incident plate surface medium as shown in the graphs of figure 16.

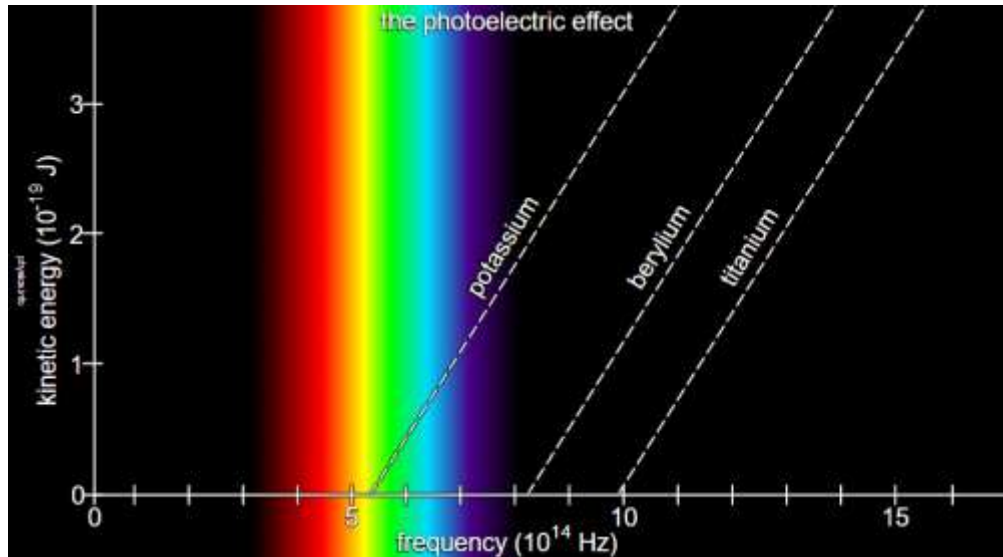


**Figure 16: Stopping Voltages to the Photoelectric Effect by Element**

Should a significant number of photons be captured by out-facing AO and CO-pole CESs, they are then be re-emitted as rebound EMR of increased wavelength (see [discussion about rebound EMR](#)). This is referred to as **Compton Scattering**, and is usually accompanied by significant numbers of photo-electrons from the direct bitron hits: thus both modified EMR and photo-electrons are emitted.

**Pair production**, like the photoelectric effect, results in the complete attenuation of the incident photon. It occurs when an incident photon with an energy level of at least 1.022 MeV (the  $\gamma$  ray range) collides with a bitron of compatible helicity, as shown in figure 17. At the impact point the photon is concertinaed and compressed against the bitron (17b), only to violently recoil and separate as a fast moving electron and positron (17c), each with sufficient kinetic energy to exit the host medium. The reverse process to pair production is electron-positron annihilation.

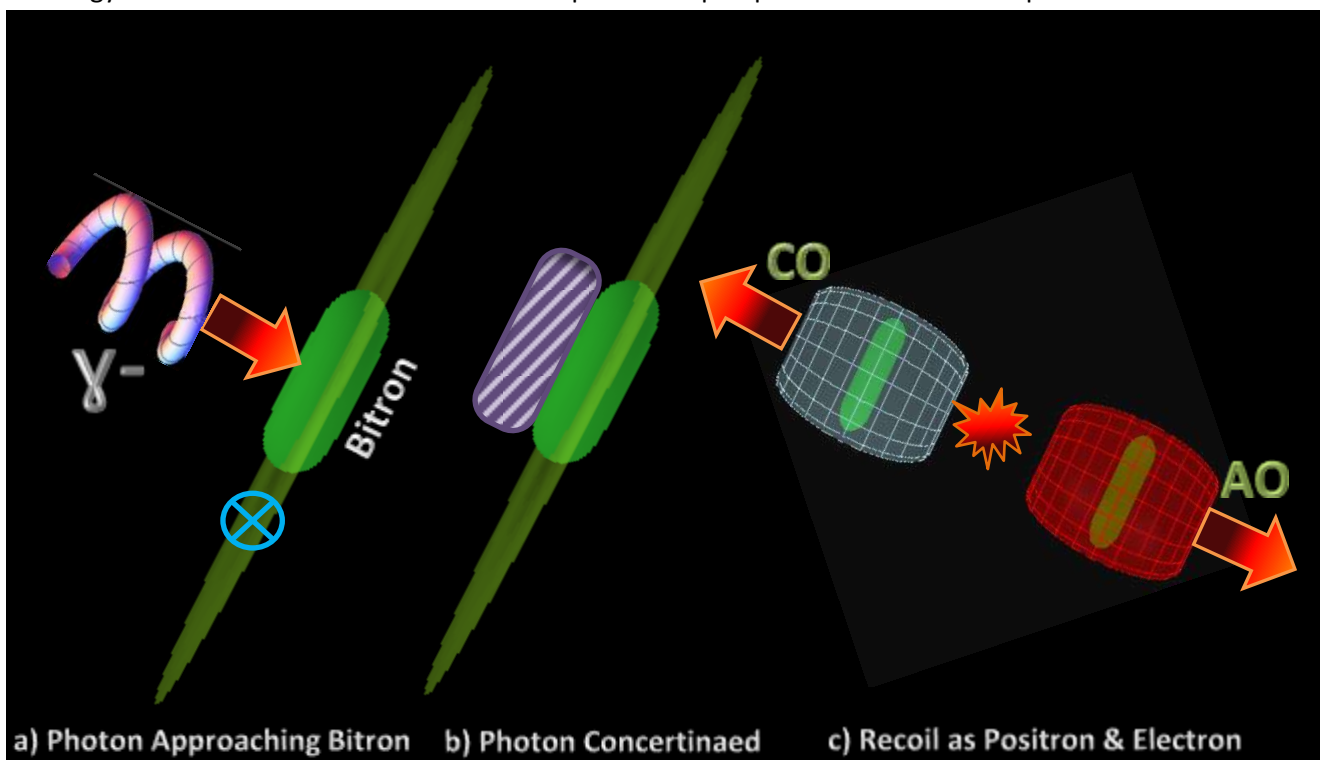
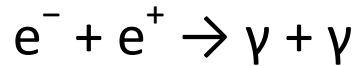


**Figure 17: Pair Production**

# Electron-Positron Annihilation

**Electron–positron annihilation** occurs when an electron ( $e^-$ ) and a positron ( $e^+$ ) collide. In a majority of cases, the result of the collision is the annihilation of the electron and positron, and the creation of gamma ray photons as



The Wikipedia diagram for the annihilation is shown in the top of figure 18 (with a Feynman diagram insert). Each electron, positron (from beta+ decay as shown) and gamma ray photon represents an energy of 0.511 MeV/c<sup>2</sup>.

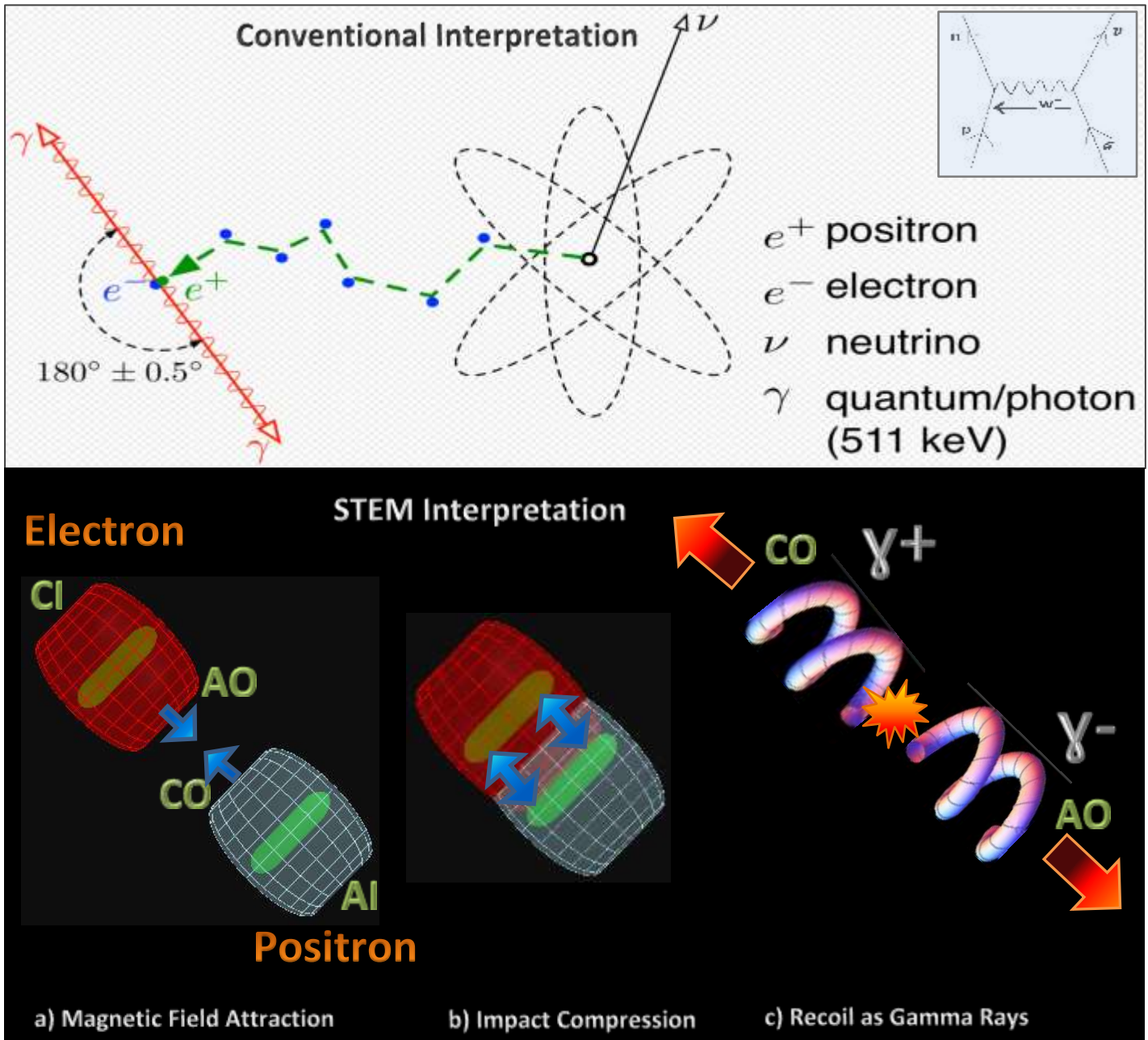


**Figure 18: Electron-Positron Annihilation**

The STEM explanation for electron–positron annihilation is represented by the bottom part of figure 18: as the electron and positron approach each other (18a), the field energy between them becomes extremely compressed (18b) and explosively de-compressing by being forced at high speed through their respective energy cores instantly converting all the energy into the helical solenoidal form of a photon, streaming away from the impact point in opposite directions (17c). The newly formed photons thus fly off at 180° to each other at close to the speed of light and with the energy and frequency of **Gamma (γ) radiation**.

The electron–positron annihilation process is used for medical applications of **Positron Emission Tomography (PET)** and for **Positron Annihilation Spectroscopy (PAS)**, which is used to the study crystallographic defects in metals and semiconductors.

# Semiconductors, P-N Junctions and Holes

A **semiconductor** is a substance, usually a solid chemical element or compound that can conduct electricity under some conditions but not others, making it a good medium for the control of electrical current. The specific properties of a semiconductor depend on the **impurities**, or **dopants**, added to it to increase conductivity in material that otherwise would be an electric insulator.

A **hole** is a fictional electric charge carrier defined with a positive charge that is equal in magnitude but opposite in polarity to the charge of a monopole electron. Holes are required by those explaining electricity in terms of monopole electrons without acknowledging the existence of positrons within matter: it is a positron substitute. **Positive holes** are required to explain electric current in semiconductor materials and capacitors. Holes and electrons are described as the 2 types of charge carriers responsible an electric current, with a hole often described as the absence of an electron in a particular place within an atom.

Although not a physical particle in the same sense as an electron (an amazing concept in itself), a hole can be passed or moved between atoms in a semi-conductor material. The process is rationalised in terms of a monopole electron and the orbital nuclear model using descriptions (and this is one of the simpler descriptions found) such as:

*Electrons orbit the nucleus at defined energy levels called bands or shells. A **hole** forms in an atom when an electron moves from the **valence band** (the shell outside the closed shells that is partially or completely filled with electrons) into the **conduction band** (the outer "cloud" from which electrons most easily escape from, or are accepted by, the atom).*

*Both electrons and holes are present in any semiconductor substance. Electrons are considered to flow from minus to plus, and holes "flow" from plus to minus. The more abundant charge carriers are called **majority carriers**; the less abundant are called **minority carriers**. In **N-type** semiconductor material, electrons are the majority carriers and holes are the minority carriers. In **P-type** semiconductor material, the opposite is true.*

But the explanation gets even more convoluted and complex. The **N-type** semiconductor has an excess of free electrons in the conduction band and the **P-type** semiconductor has an excess of holes in the valence band. An N-type semiconductor is considered to carry current mainly in the form of negatively-charged monopole electrons whereas a P-type semiconductor carries current via positive hole migration in the opposite direction to electron movement.

When N-doped and P-doped semiconductors are placed together a **P-N Junction** is formed, due to dopant ionisation free electrons are generated on the N-side, so creating **positive ions**. These free electrons magically migrate (diffuse) into the P-side, so creating **negative ions** on the P-side.

Once **equilibrium** has been reached, the zone in which ionisation and electron movement has taken place is called the **depletion layer** (or Space Charge Region as shown in figure19), which, like Trump's wall, presents a barrier for further electron migration. The ion-induced emf across the barrier is variously called the built-in voltage, junction voltage, barrier voltage or contact potential.

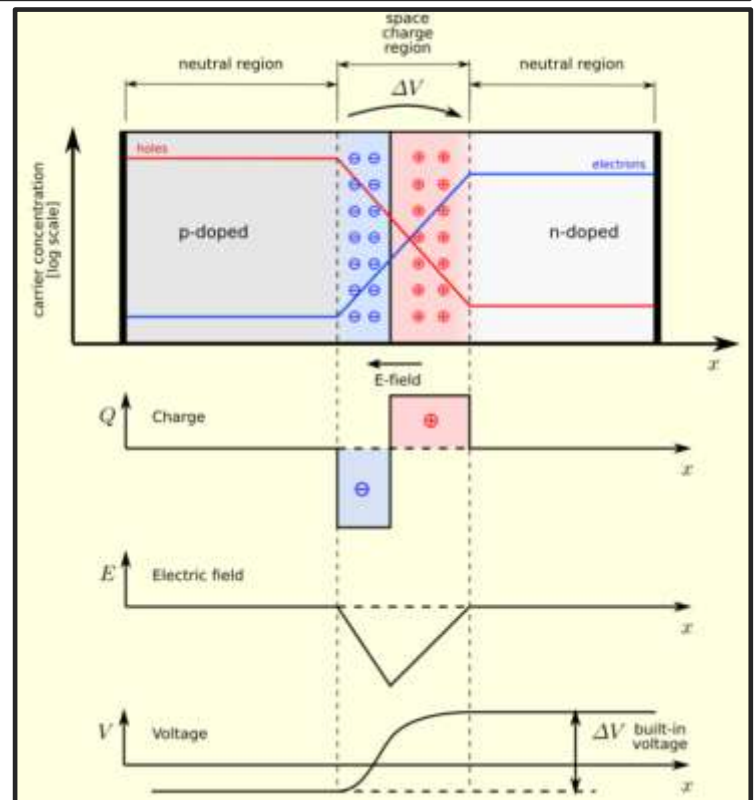


**Figure 19: The P-N Junction**

The Off/On switch nature of the P-N junction is achieved by applying a small reverse bias voltage across the junction ensuring that no further electrons can move across the junction (Off mode), or a forward bias allows electrons and compensating holes to move across the junction in opposite directions with very little resistance (On mode).

The monopole electron and the Orbital Nucleon model does not have an explanation for the relationship between electric and magnetic fields, and because of a lack of recognition of the existence of positrons within matter, has difficulty in describing how electric currents work to the extent that fictional positive holes have to be invoked for semiconductor circuitry. This represents quite a sad state of affairs.

The STEM explanation of P-N junctions and related semiconductor circuit components is not full of holes. It is quite straight forward; is fully compatible with the STEM explanation for electric currents, electromagnetic fields and atomic bonding as presented in parts 1 and 2 of this series; and the explanation mainly relates to chirality and geometry. But first we need to have a look at the manufacturing process and nature of silicon wafers and those important dopants.

A thin slice (between 160 to 300  $\mu\text{m}$  thick) of **crystalline silicon** of high purity (99.999999%), and called a **wafer**, is the substrate used to build semiconductor circuitry and to manufacture solar cells. Although wafers can be created by solid state dopant diffusion, commercially they are produced in bulk using the Czochralski process (named after Polish chemist Jan Czochralski who invented the technique). Both manufacturing processes ensure that the silicon atoms' Z-axis (see figure 20b), lies close to parallel to the wafer slice plane, and this geometry is important to the P-N junction.

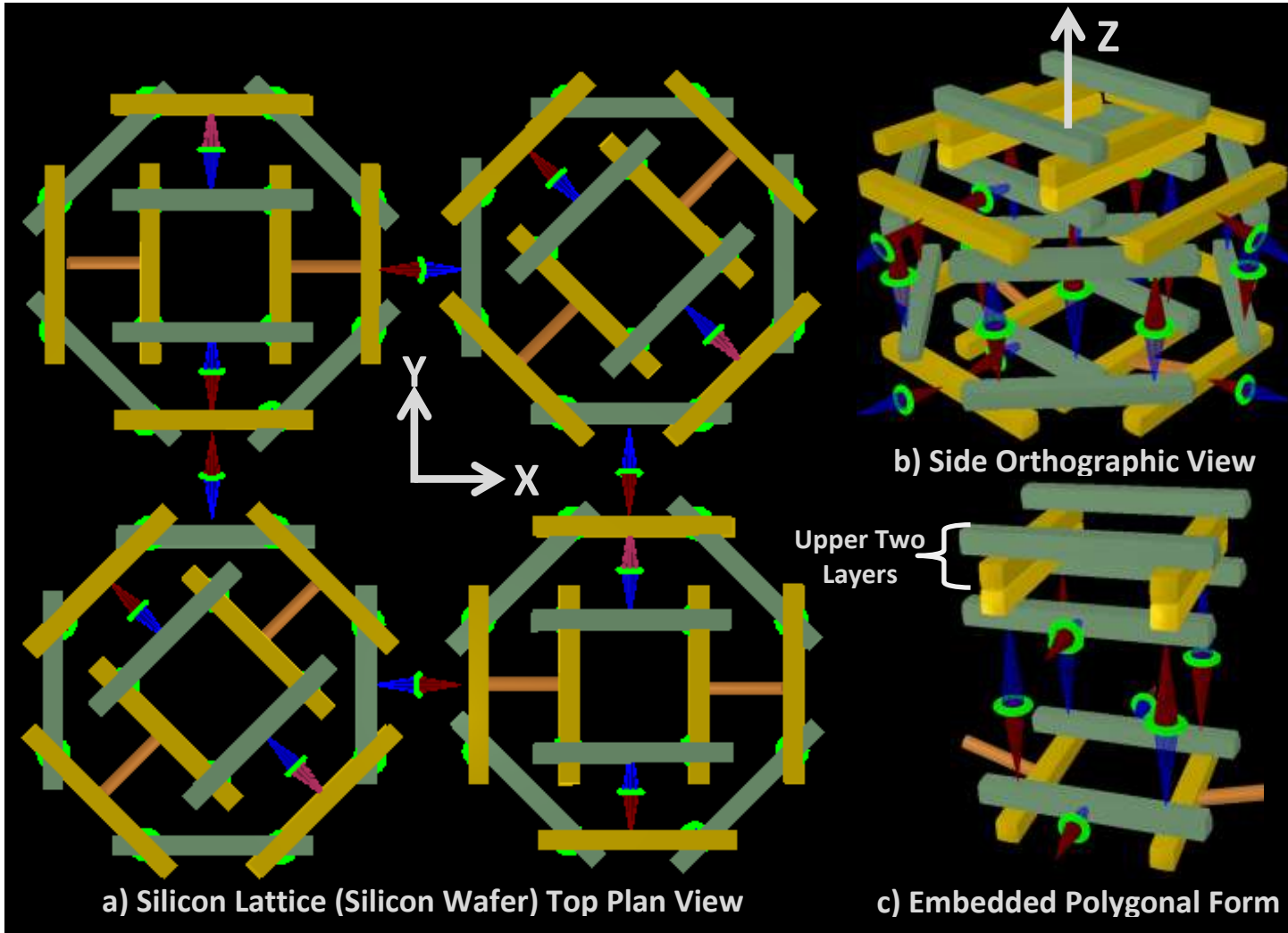


**Figure 20: Silicon Atom and Wafer Structure and Orientation**

All nucleon layers within silicon atoms are complete, with all their swivel quarks either participating in inter-atom bitron bonds or immobilised by offset bonds. Thus, in a silicon wafer, silicon atoms have no unrestrained swivel quarks that can give it a positive or negative charge (i.e. they are non-ionic) or be available to capture and hold free electrons or positrons. They are stable, electrically neutral, void of associated free electrons or positrons, and hence the need for dopants to supply electrons and positrons. So far this is in full agreement with the conventional Science view.

For Czochralski silicon, measured quantities of dopants are added to a silicon dioxide molten mix: commonly Phosphorus for n-type and Boron for p-type semiconductors. Within the melt, the silicon and oxygen bitron bonds within the silicon dioxide break down, releasing oxygen and lots of excited electrons and positrons, many of which attach to available swivel CESs within the dopants: this process warrants further explanation.

Whereas silicon is electrically neutral, Phosphorus-31 has the same structure as silicon but has L-form nucleons in its **upper neutron layer**: 1 proton and 2 neutrons (see figure 21c). These nucleons create a swivel e-quark, which means that Phosphorus-31 is a negative ion capable of capturing one or more electrons as shown schematically in figure 22a.

Similarly, Boron-11, produced by the decomposition of Diborane at high temperatures, has a tetragonal form (see figure 21a). It also has of 1 L-form proton and 2 L-form neutrons attached to its **upper proton layer**, which creates a swivel p-quark, (see figure 21b), so forming a positive ion that is capable of capturing one or more positrons.

In the Czochralski process, as the molten silicon mix slowly cools, both P-31 and B-11, which have side bonding capabilities compatible with that of silicon, take up random positions within the developing silicon lattice with their attached electrons and positrons parallel to the Z-axial direction of the silicon atoms (see in figure 20) in the wafer.

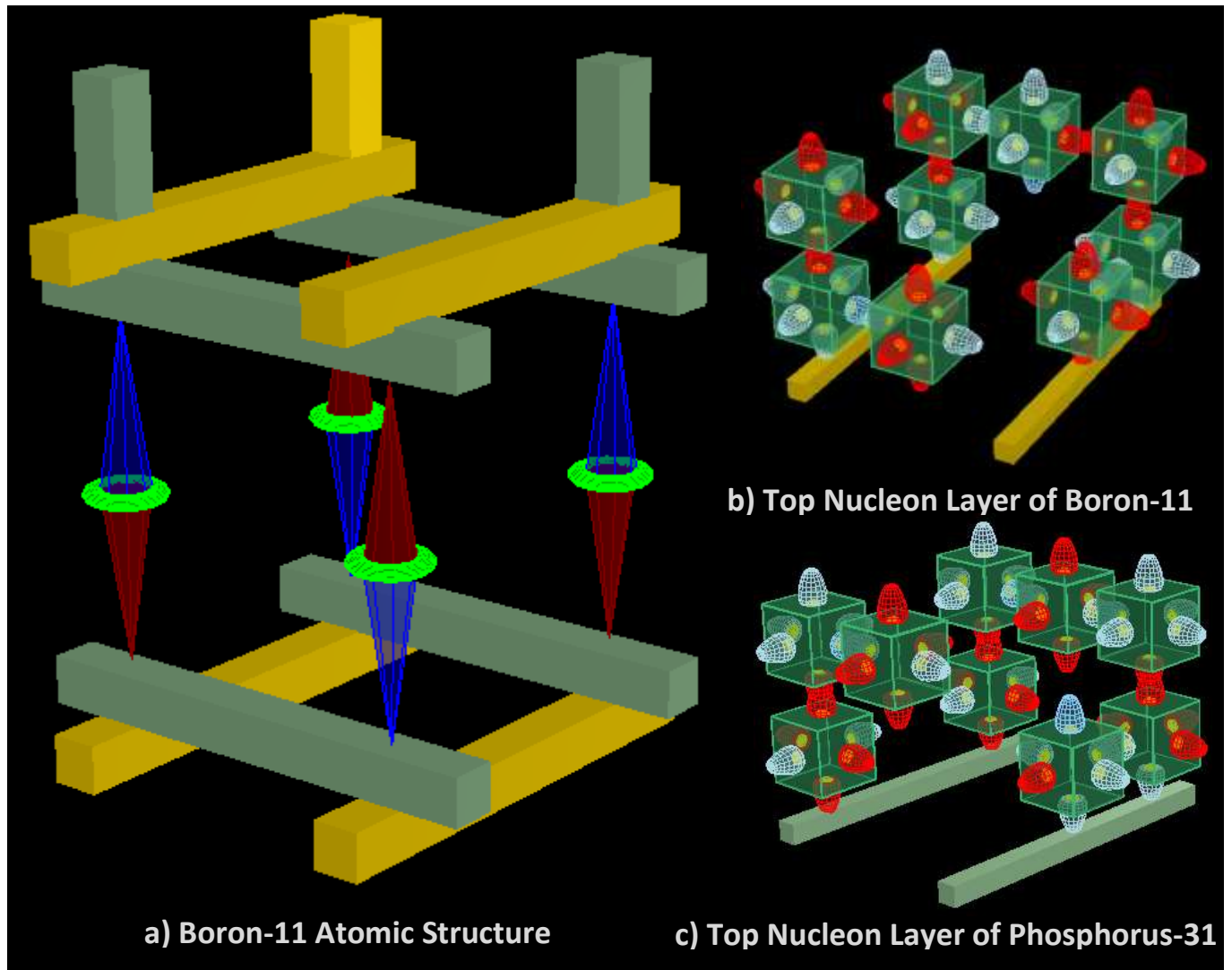


**Figure 21: The Structure of the Dopants**

As the silicon melt cools, the dopants embedded within the silicon wafer structure all point in the same z-axial direction, as in figure 22a (dopant atoms are represented as amorphous spheres). As the dopant atoms become de-energised, they release their attached electrons (from Phosphorus-31) and positrons (from Boron-11) as in figure 22b. Normally it would be expected that these released electrons and positrons would revert to neutral bitrons (figure 22c). However within the depletion zone this is not the case.

Because the z-axis of all the atoms in the wafer are approximately perpendicular to the p-type and n-type abutment surface, their upper-layer spin quarks randomly face towards or away from the abutment surface as shown in figure 23a. Thus, due to geometry, only those dopant atoms near to and facing the abutment surface (there is a tolerance of about  $\pm 45^\circ$  which caters for oblique abutment joins) can release electrons (for p-type) or positrons (for n-type) into the depletion zone. Further away from the depletion zone the orientation is randomly facing towards or away from the abutment surface.

Thus, within the depletion zone all the electrons on the p-doped side all have their AO poles facing the abutment surface, the positrons their CO poles facing the opposite direction on the n-doped side. These orientation differences between the depletion zone and the rest of the wafer can best be appreciated from the bitron representation of figure 23b. The electrons and positrons in the depletion zone also fall between the negative charge of the p-type anions and the positive charge of the n-type cations: thus, as they all have the same spin direction, they start to migrate across the abutment surface as a micro current until equilibrium is established. (figure 22e). This is a simple source-sink micro electric current that is analogous to the charging phase for a capacitor (see Part 1).

Even after equilibrium has been reached, the net ionic charge sustains a weak polarisation of electrons on the n-type side and positrons on the p-type side in the depletion zone, whereas those outside the depletion zone revert to neutral bitrons, requiring an external emf to polarise them so as to re-form into electrons and positrons.

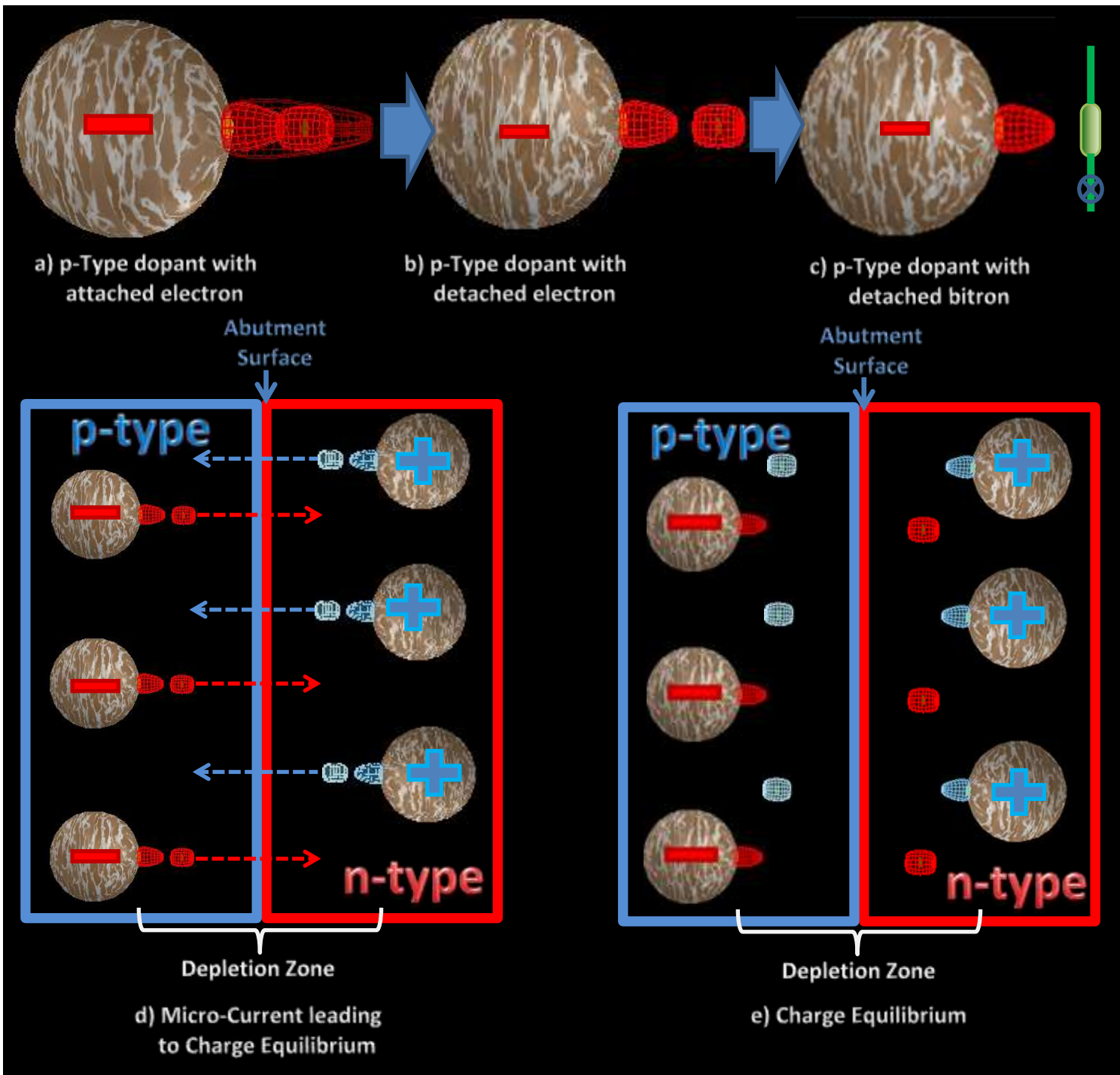


**Figure 22: Effects of Dopant Ionisation**

Outside the depletion zone and facing the abutment surface there are approximately equal numbers of clockwise and anti-clockwise spin bitrons grouped into sparse strands as in figure 23b. These strands are capable of forming an electric current flowing in either direction dependent on the direction of the externally applied emf.

The story is different in the depletion zone where the strands are composed of bitrons with the same spin direction. Thus the depletion zone can only support current flow in one direction. When a forward bias emf is applied across the junction (figure 23c) a current readily flows across the junction, but when a reverse bias is applied the current cannot flow across the depletion zone, which acts as a break in circuit and represents an off-switch.

Even without applying a reverse bias, the emf (the **built-in potential**) generated by the ions is sufficient to keep the depletion zone bitrons polarised without current flow; a reverse bias simply reduces the depletion zone electrons and positrons to bitrons, ensuring no current leakage whilst in off mode.

This very simple explanation does not requiring the creation of fictitious holes and associated gobbledygook. It is an explanation that is fully compatible with the STEM explanation for electricity, capacitors, atomic structure and ionisation. It has continuity and simplicity, and a consistency spanning many areas.

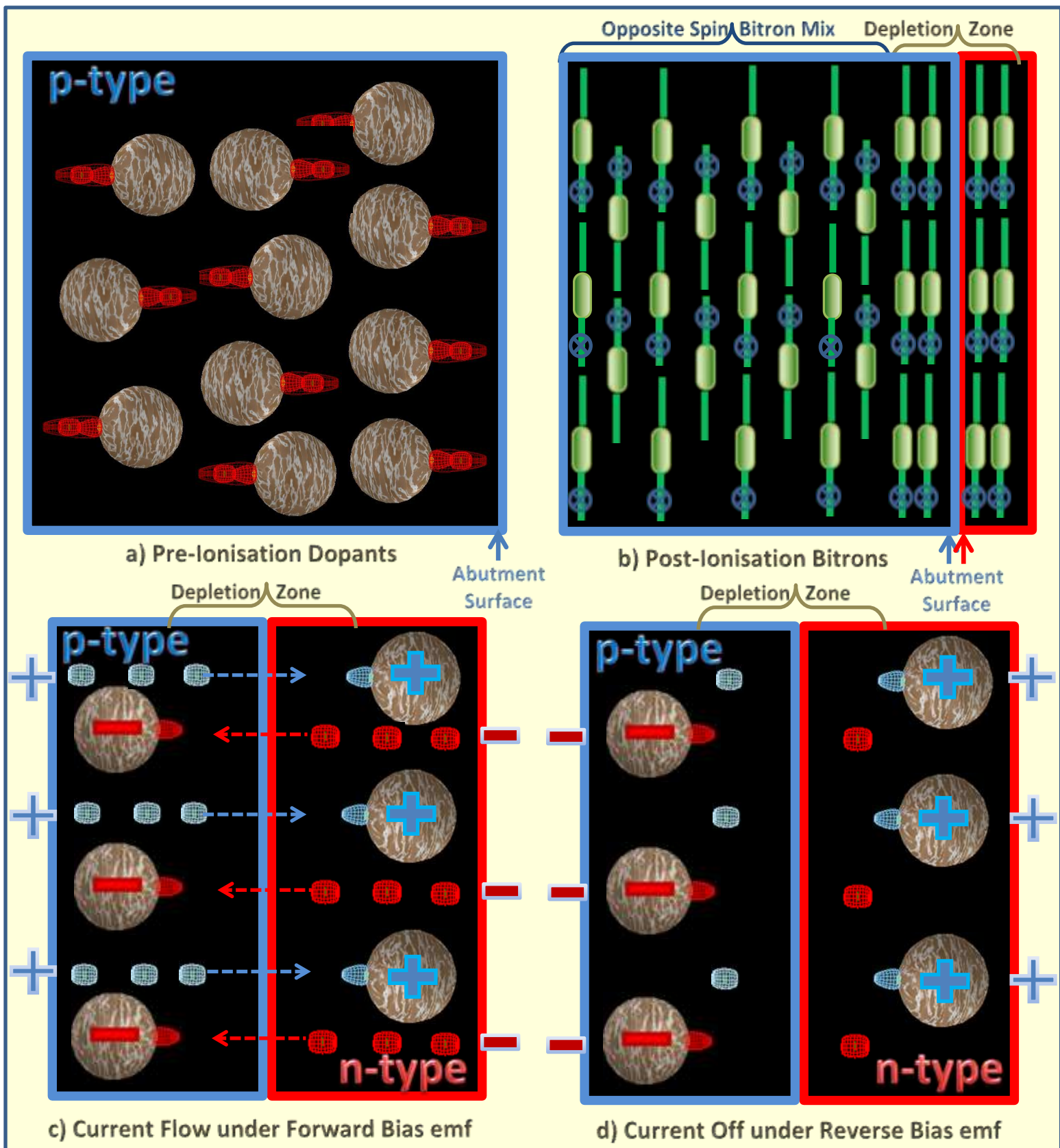


Figure 23: Boundary Effects and Forward/Reverse Bias Effects

In way of a summary, within the depletion zone, due to geometry, all the electrons and positrons from the dopants have the same spin direction, which means that they can only support an electric current in one direction, as induced by a forward bias emf. Electrons and positrons deposited within the semiconductor wafers outside the depletion zone contain bitrons with a random mix of clockwise and anti-clockwise spin, and thus can support a current in both directions. When a forward bias is applied across the P-N junction current flows (the ON setting), but not when a reverse bias is applied (the OFF setting) due to the depletion zone.

# Plasma and Cosmic Radiation

**Plasma** is formed by super-heating matter, which causes electrons to be stripped from the atomic structure to yield a mixture that is rich in electrons and ions. Over 99% of the matter in the visible universe is believed to be plasma. An important source of plasma formation in space is **photoionization**, wherein photons from stellar EMR are absorbed by an existing gas mixture, causing electrons to be emitted.

Closer to Earth, lightning, naked flames, welding arcs, neon/fluorescent tubes, neon signs, plasma (some TV and computer screens), plasma lamps and globes involve the generation of plasmas; and the Earth is surrounded by a dense plasma called the **ionosphere** and impacted by the Sun's solar wind plasma.

Plasma can also be created in the laboratory by super-heating a neutral gas or subjecting it to a strong electromagnetic field to the point where it is ionised. At lower temperatures radiant EMR energy is acquired and managed by the energy transfer and balance mechanisms as described [earlier](#).

The temperature and degree of chaotic buffeting within a gaseous mix increases as the energisation levels increase, and bitrons start being released from external bitron bonds as a fast moving electrons or positrons, greatly increasing the electrical conductivity of the mix. This early stage ionisation is accompanied with the generation of extensive long-range electromagnetic fields and production of gamma radiation from electron-positron annihilation collisions.

As the energisation continues to increase, increased levels of external bitron bonding fail and the plasma mix becomes increasingly ionized. For Hydrogen ionization starts at about  $7,000^{\circ}\text{K}$  and by around  $10,000^{\circ}\text{K}$  it is completely ionized.

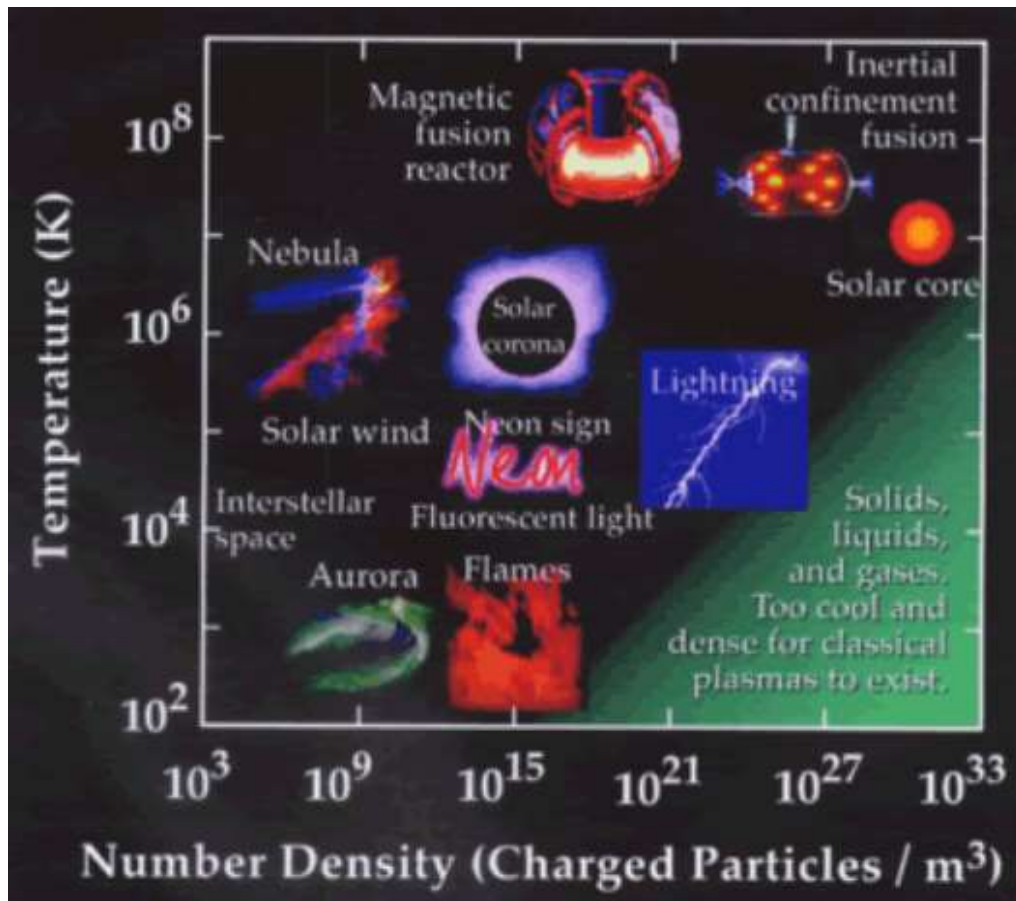


**Figure 24: Plasma Temperature/Density Distribution**

When temperatures rise to well above the  $10^4\text{K}$  range, such as achieved by active stars, the bitron bonds supporting nucleon layers within atoms (i.e. atoms more complex than Hydrogen) start to fail, facilitating the separation of nested polygonal forms and the creation of atoms of lower atomic number. The very fabric of the original compounds has commenced to break down, with any semblance to the original atomic structures being lost. Cooling of the plasma cloud would at this stage would result in a completely different mix of atoms and compounds.

Should energisation continue even further, nucleon layers would be further separated with the destruction of any remaining inter-layer bitron bonds, and the layers then broken down into their component nucleon and/or quark parts: such utter destruction and decomposition most likely only occurs in the crush within the bowels of a black hole or collapsing neutron stars.

For Hydrogen, the most elementary and widespread form of plasma in the universe, the ionization process takes place from about  $7,000^{\circ}$  K, with the bitron bonds of Hydrogen molecules being stripped away, creating a mix rich in electrons, positrons and protons (hydrogen nuclei). At this stage some interesting things start to happen:

- Firstly, the destruction of hydrogen molecule bitron bonds mean that the in and out energy flow of protons is not restricted. Thus energy no longer accumulates within out-facing CI-pole or AI-pole CESs within the rising number of protons. As the protons (and any free neutrons) no longer emit EMR Hydrogen drops out of emission spectra for the plasma mix, with any spectral lines being attributable to contaminants.
- Secondly, because highly energised free electrons and positrons abound, protons are being toggled into neutrons via  $\beta+$  decay (see earlier) and then back again into a proton via  $\beta-$  decay. This ongoing circular process generates a large number of beta rays, neutrinos and anti-neutrinos.
- Thirdly, the ongoing toggling of nucleons between proton to neutron and back again generates a mix of free protons and neutrons in close proximity, which allows them to combine and form new atoms, principally Helium, which, in such a highly energised environment, present as alpha radiation.

**Cosmic radiation**, the high-energy particles arriving from outer space from distant galaxies, consists mainly of protons (89%), Helium (10%) and a mix of heavier nuclei (about 1%), plus abundant levels of high-energy neutrinos, anti-neutrinos and gamma radiation: a content compatible with that of a completely ionized Hydrogen plasma mix.

## Spin and the Orbital Nuclear Model

Central to the STEM approach is that all concentrated energy sources (CESs) have spin, and that low level electromagnetic energy spirals around them in synch with their spin, with the circular divergent and convergent flows presenting as positive and negative charge electric fields, and the lengthwise flow presenting as a magnetic field. As electric and magnetic fields are formed by the same electromagnetic energy, they are only differentiated by their flow pattern and characteristics associated with those patterns. With STEM there is no need to balance the notional positive and negative point charges to achieve electrical neutrality: only magnetic moments need to be accounted for.

For the conventional Science approach based upon an orbital nuclear model for atomic structure, the combination of charge and spin has proven to be more problematic. In the early 1920's the Standard Model consisted of a Bohr-styled model for atomic structure consisting of negatively charged electrons orbiting a positively charged nucleus. **Orbital angular momentum** was accounted for by integer quantum numbers, but it was soon realised that the orbiting electrons possessed magnetic moments associated with their axial spin, called **intrinsic angular momentum**. In the late 1920's Paul Dirac's equations, which factored in relativistic theory, allocated fermions (including electrons) quantum spin  $1/2$ ,  $3/2$  etc. to cater for intrinsic angular momentum, with anti-particles having a corresponding negative half spin number.

The **Stern–Gerlach experiment** is used to illustrate that an orbital electron possesses intrinsic angular momentum due to electron spin. The experiment involves sending a beam of silver atoms through an inhomogeneous magnetic field and observing their deflection as shown in figure 25.

Due to random thermal effects in the oven used for the experiment, the magnetic dipole moment vectors of the silver atoms are considered to be randomly oriented in space. Based on classical physics theory, a continuous spread of the atoms in the z direction corresponding to the random spread of magnetic moments could be expected (a lip-like pattern filled with atom hits as shown in the top-right insert of figure 25): instead the experimental results had no central hits resulting in the open thin-lip distribution as shown.

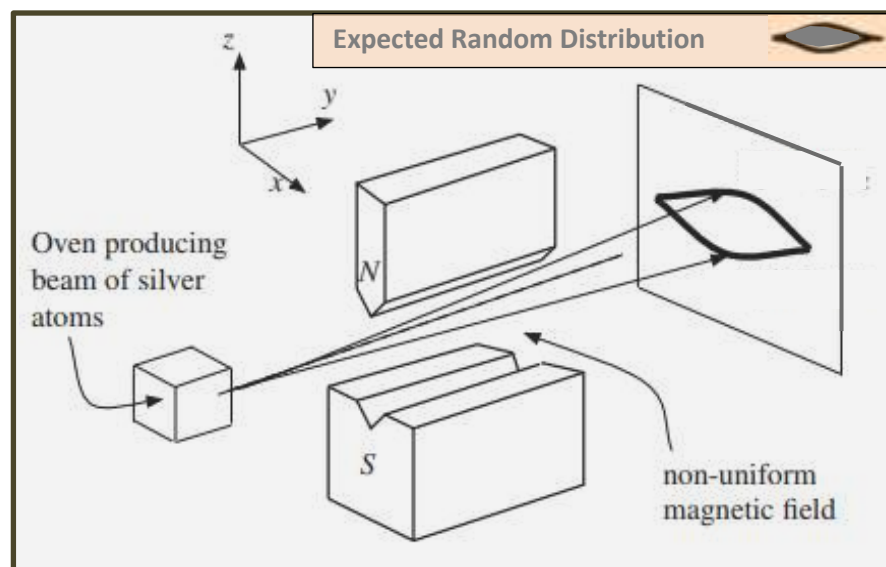


**Figure 25: The Stern–Gerlach Experiment Setup**

Originally the thin-lip distribution of the atom stream was interpreted as being due to integer quantised angular momentum as per the quantum theory that then (1922 to 1925) existed. Upon the arrival of Dirac's equations in the late 1920's, the experimental results were re-evaluated and conclusions changed: the deflection pattern was now explained in terms of the intrinsic angular momentum of orbital electrons. According to the orbital model, silver atoms have one unpaired 5s electron, with all others being paired. Thus, as the 5s electron is considered to be in a zero orbital-derived angular momentum state, its quantum spin-1/2 results in an up or down state, resulting in an even splitting of the electron stream in the z direction.

With a magnetic susceptibility of  $-2.27 \times 10^{-9} \text{ m}^3/\text{Kg}$  silver atoms are diamagnetic. STEM can explain silver's diamagnetic nature in terms of the bond geometry, but that is only a side issue when discussing this experiment.

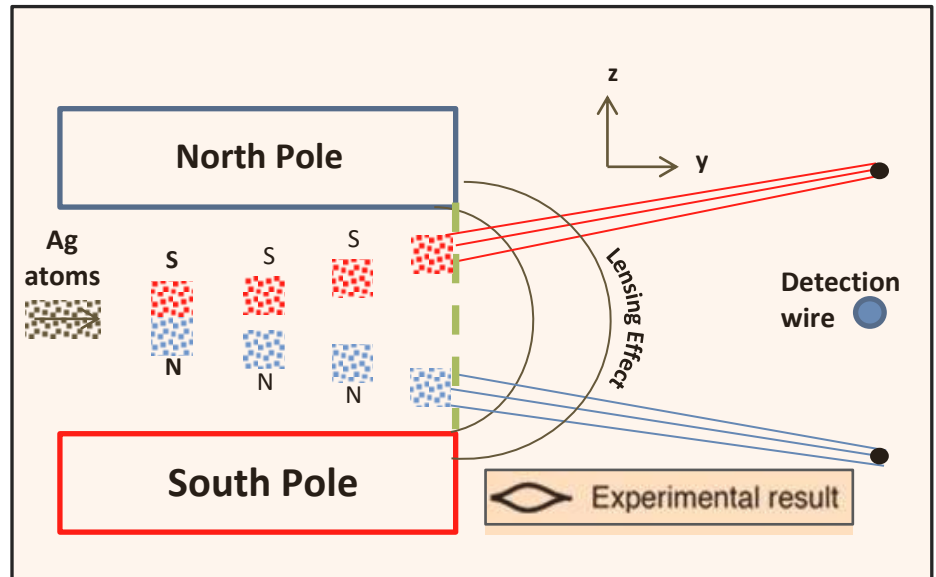


**Figure 26: The Stern–Gerlach Experiment Deflection Pattern**

In an inhomogeneous magnetic field the unrestrained atoms will quickly rotate to align themselves in the magnetic field so that their magnetic fields are in the opposite direction so as to oppose the applied field. Such alignment will cause the silver atoms to be attracted to the closest magnetic pole as shown in figure 26. Also due to mutual magnetic attraction they would move closer to each other while moving as two distinct populations towards the relevant applied field poles.

The result would be a fairly concentrated lens-like distribution band with no atoms centrally, thus producing an open lip-styled pattern. Also, in a manner not dissimilar to the optic focusing effect of a convex lens with light, the convex shape of the outer magnetic field at the atom exit-end of the magnet (dashed olive-green line in figure 26) would have a far-field lensing effect causing the atoms to converge further into thinner lines as observed.

## The Pull of Gravity

Small, almost insignificant amounts of energy is being continually lost or leaked from the swirling electromagnetic fields of CESs, electrons, positrons and photons; for bitron bonds the amount of energy lost is more significant. Although some of the 'lost' energy is absorbed by other close-by concentrated energy forms, the rest accumulates as a very weak pool of 'stagnant' energy around the host object from which it escaped. STEM contends that low-level leakage energy accumulates **atmosphere-**like around all normal matter: thus it has been called an **Enersphere**.



The inter-quark connectivity of nucleons provide them with an **energy capacitance** (explained in more detail in the next chapter) that creates a mismatch between the funnel-like suction action of their energy in-flow CESs (CI and AI) and out-flow, which results in a small net positive pull on the enersphere immediately surrounding the host object. STEM contends that the resultant minute inwardly-directed force, summed over the billions of nucleons (1 litre of water contains approximately  $2 \times 10^{27}$  or 2 octillion nucleons) within an object, is the pull of **Gravity**.

The more nucleons that an object contains, the larger its enersphere would be and the more cumulative in-flow pull it would have, so increasing its gravitational pull and its **mass**. Thus it is the total number of nucleons within an object that dictates its energy content and its mass (implicit in  $E=mc^2$ ), and, in relation to Earth, it is the size of an object's enersphere and its location within Earth's enveloping enersphere that dictates its **weight** (mass x G).

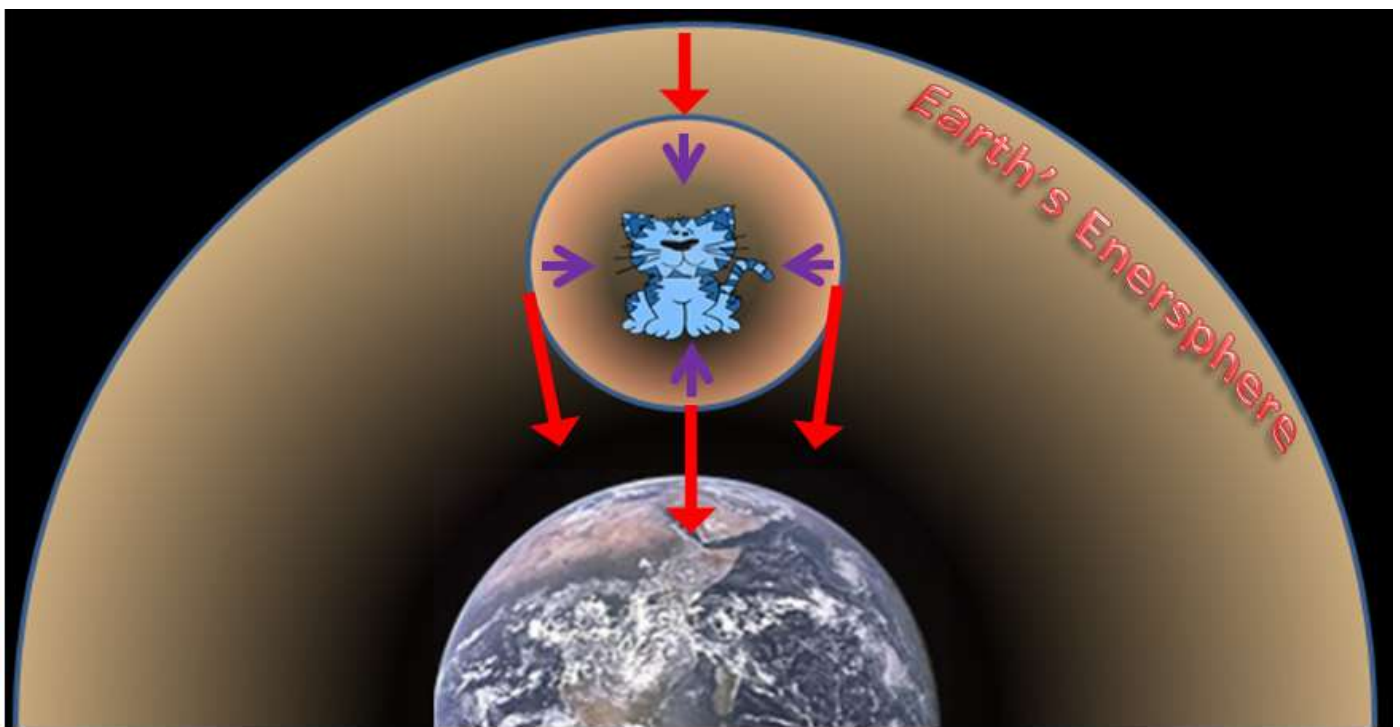


**Figure 27: Model for Earth's Gravity**

Figure 27 represents a cat sitting with its enersphere fully within the Earth's enersphere. The purple arrows show the direction of the forces pulling the cat's enersphere towards the cat, and the red arrows the considerably greater forces pulling the cat's enersphere towards the surface of the Earth. The cat is heading earthwards, free falling under the influence of Gravity.

The depiction of figure 27 is idealised because the shown bubble boundary surfaces do not exist - when one object's enersphere overlaps another's they simply merge into one, with the energy levels of each enersphere adjusting appropriately to the other. The suction-like pull of the in-flow CESs within each object (here the cat and Earth) would continue to pull energy from the resource-in-common, their merged enerspheres, with the forces acting in the zone of the cat being similar to those shown, as would be their nett effect.

At the macro level, enerspheres of large bodies extend well into space (e.g. the Moon, Earth, the Sun, the stars and galaxies) intersecting and acting together to create Gravity pull between systems. The huge, far reaching enerspheres of large objects in space suggests that their enerspheres could possibly be in expansion mode, albeit slowly. It is difficult to imagine any region of space without enersphere energy, even if it is only from the vapour trails of photons.

As large scale cosmological systems approach each other, their enerspheres merge causing an increase in enersphere bulk and thus the magnetic pull of each towards the other. For merging systems such as **neutron stars** or **black holes**, a spin embrace results (see figure next to this chapter's header) which climaxes in a rapid compression of their combined enerspheres leading to a massive explosion of compressed energy and consequential **Gravity waves**.

Enerspheres are a remarkable bi-product of the way energy combines to make atoms and of atoms to make matter. STEM contends that the pull of Gravity is due to the retrieval of enersphere energy rather than being a mysterious external force or a result from the warping of **space-time**. It is a model that applies equally well both at the micro scale (e.g. Gravity forces applying to objects on Earth) and macro cosmological scale.

**Historical Note.** René Descartes, famous for his philosophical assertion *cogito ergo sum* ("I think, therefore I am"), in 1644 proposed that **aether**, the medium then considered to separate objects and matter (cf. space), is filled with vortices whose **inward pressure** is 'nothing else than Gravity'.



Equate **Descartes's vortices** to in-flow CESs within nucleons and consider the **aether** to be the enersphere energy surrounding matter, then, **philosophically speaking, Descartes's 375 year-old explanation for Gravity was not far removed from that of STEM.**

(It should also be noted that, at this stage, STEM does subscribe to the notion that aether is the substance or medium in space that supports the propagation of EMR in a wave form.)

# Issues Related to Quark and Nucleon Size and Mass

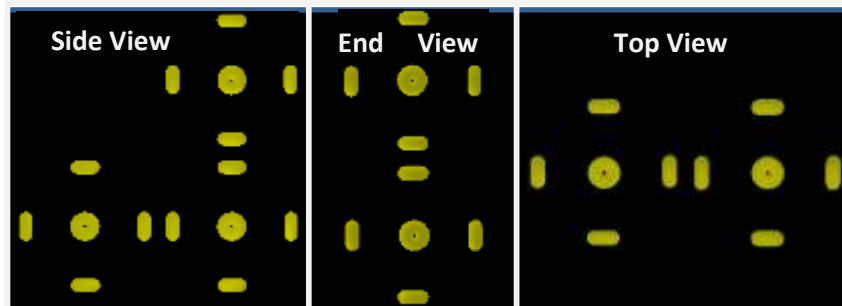
This chapter looks at some problems and issues that are associated with the size and mass of quarks and nucleons. It also introduces and describes a third type of nucleon structure: the **triangular-form nucleon**.

One major Physics problem is the discrepancy between the mass of  $2.3 \text{ MeV}/c^2$  attributed to up quarks and  $4.8 \text{ MeV}/c^2$  to down quarks: these values are at odds with the mass of  $938.3 \text{ MeV}/c^2$  attributed to protons, which are made up of 1 down and 2 up quarks (UDU), and  $939.6 \text{ MeV}/c^2$  to neutrons (DUD). STEM contends that energy inflows and outflows are reciprocal (i.e. balanced) and unrestrained for free up and down quarks and thus they have no net pull on the surrounding enersphere. Free up/down quarks do not contribute to Gravity and thus, although they have energy (6 CESs), they have no mass: place any 3 up/down free quarks on one side of a cantilever balance and a nucleon on the other side, and the balance would tip towards the nucleon side as if the free quarks were not there. It is totally misleading to attribute free quarks with mass estimates and then try to use them in a meaningful way.

When joined to form a nucleon, 4 CESs (of the available 18 CESs) form the 2 inter-quark bonds holding the quarks together, which provide a dynamic energy transfer and balance system between the quarks. Rather than being immediately purged via out-flow CESs, some of the drawn-in enersphere energy is pumped around the nucleon to be adsorbed by the energy core of a CES, lost to the enersphere (e.g. via the heavy energy field losses associated with bitron bonds), or simply gradually accumulates within the nucleus. The net result is that CES energy in-flow, and the associated pull on the enersphere, exceeds CES energy out-flow by a small amount, and that extra inwards pull on the enersphere contributes to Gravity and provides nucleons with mass.

Each nucleon in each atom contributes equally to Gravitational pull and an object's mass. Thus the total number of nucleons within an object dictates its mass ( $m = \sum m_n$ ): and because each nucleon contains the same amount of CES core energy, the equation  $E=mc^2$  follows. As it would be rare for a nucleon layer to be able to reach its energy capacitance limit via accumulated enersphere energy alone, energy capacitance limits are typically exceeded by energy acquired from external sources and/or an energised environment. The excess energy acquired is then released as EMR emissions and/or via the loss and re-building of bitrons within external bitron bonds.

Another Physics problem relates to the proton's size: [the latest \(2010\) estimate of the proton's radius](#) was deduced (not physically measured) to be 0.842 fm from electron-proton scattering experiments. This is an amazingly small size because, assuming a radius of 2.82 fm for an electron, it results in a proton radius about  $1/3^{\text{rd}}$  of that of an electron, or the electron being about 38 times the size of a proton by volume. The possibility of (relatively) large electrons whizzing around the diminutive nucleus of an atom creates a huge dilemma for Physics world. The problem has arisen because a proton has been modelled as a fundamental particle with a central spherical energy core. STEM, on the other hand, contends that nucleons consist of a 3D array of 18 CESs, and that the interference patterns observed result from interference with a sparse array of CESs (see diagram right), and the equations returned an unrealistic and ridiculously small estimate for proton radius based upon an incorrect model (which is different from the equations being erroneous).



Although the radius of the electron used in the previous paragraph was 2.82 f m, electron radius has not been determined to any degree of confidence, being [variously estimated to fall within the range of  \$3 \times 10^{-11}\$  to  \$10^{-18}\$  m](#). With such disparity between the claimed sizes of protons and electrons it seems reasonable for STEM to deduce the size.

The dimensions of atoms are reasonably well established and seem to be a good starting point from which to deduce the size of nucleons and electrons. The 2<sup>nd</sup> smallest atom, and one of the structurally strongest, is He-4, which was addressed in part 2 of this series. The orbital nuclear model represents the helium atom as an amorphous spherical nucleus surrounded by a single sphere  $1s^2$  orbital shell with an orbital diameter of about 60 pn (1 PicoMetre =  $10^{-12}$  m). The STEM He-4 atom has a cubic form consisting of 2 overlapping pairs of I-form protons and neutrons as in figure 28b. The 60pn diameter corresponds to an I-form nucleon length of between 42 (width measured diagonally) and 60pn, with 45pn being a reasonable compromise. Thus the cubic form of up/down quarks would have side dimensions of 15 x 15 x 15 pn inclusive of the inter-quark bond gaps. A 15 x 15 pn quark face could comfortably support 2 to 8 pn diameter CES energy core diameter, with a 5 pn diameter representing a reasonable compromise. It would then seem reasonable for a bitron formed between a pair of 5 pn diameter CESs to have a diameter in the order of 3 pn.

Based upon simple geometry and a bit of logical reasoning, should a nucleon be considered to be an oblate spheroid,

it would have major axes (diameter equivalents) in the order of 30 x 30 x 15 pn; a CES a diameter of about 5 pn; and an electron a diameter of about 3 pn ( $3 \times 10^{-12}$  m). Note that the estimated electron size of  $3 \times 10^{-12}$  is about 1000 times larger than the 2.82 fm value used above, but it still lies well within the published size range  $3 \times 10^{-11}$  to  $10^{-18}$ .

As mentioned in the chapter '[Plasma and Cosmic Radiation](#)', cosmic radiation from distant galaxies consists mainly of protons (89%) and Helium (10%). He-4 has a very strong structure which allows it to survive violent aggressive environments. However, L-form nucleons are not so robust and would soon be broken down and destroyed. STEM considers that the Triangular-form (T-form or  $\Delta$ -form) nucleons (see figure 28c and 28d), which are entirely inter-quark bonded and thus quite strong and robust, would be the prevalent nucleon form within such environments.

In the highly energised, volatile and abrasive environment causing the generation of cosmic radiation, the super-tough T-form nucleons and He-4 atoms would act like steel pebbles in a grinding mill, destructively reducing larger atomic structures into single transient quark remnants, 2-quark mesons and more T-form nucleons, and releasing a lot of additional energy. Not all T-form nucleons would survive intact, with many being damaged by the turmoil to become a more vulnerable L-form nucleon that can inter-link with other L-forms to generate more He-4 atoms.

It is also quite possible that most nucleons attach to the outer layers of atoms as T-form nucleons, and are only reduced to L-form nucleons by battering and being battered by adjacent nucleons. For sparsely populated outer nucleon layers, many nucleons could still remain as intact T-form nucleons rather than L-form. The 'X' symbols of figures 28c and 28d indicate the only CESs that do not flip during nucleon-type conversion.

The Helium-4 atom was described in part 2 of this series as having with 2 internal bitron bonds. It is highly unlikely that such bitrons would form, and should they form, it is unlikely that they would survive for long in the highly energised environment in which He-4 atoms formed. They were included in the part 2 description mainly to maintain some level of compatibility with the orbital nuclear model: the author considered it too drastic to describe He-4 as electron-free. But bitron bonds are neither needed to keep the He-4 nucleons apart nor to provide compressive strength, whereas the orbital nuclear model needs electrons orbiting a positively charged nucleus. For similar reasons related to minimising new concept and information overload, early mention of T-form nucleons was also avoided.

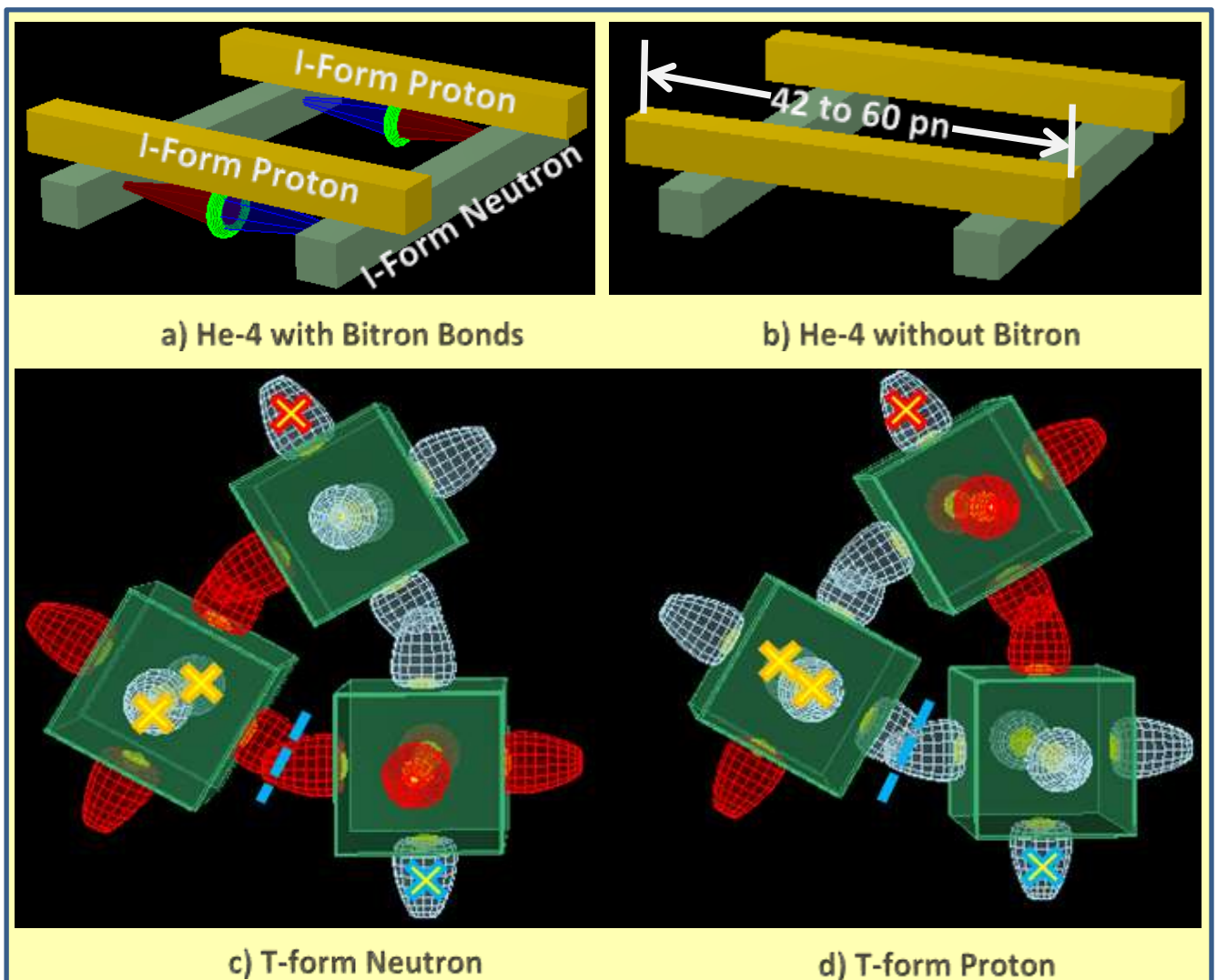


**Figure 28: Helium-4 and T-form Nucleons**

# Conclusions

The pragmatic energy-centric approach to atomic structure, as developed in this series of papers, has been based upon a **toroidal** model for electrons, positrons and CESs; and a **helical solenoid** model for photons. The resulting atomic structure model is significantly different to those of conventional Science's orbital nuclear (or Rutherford) model, and provides seamless practical explanations for many physics and chemistry related phenomena, including:

- The physical characteristics of elements
- Different allotropic forms of elements
- Bonding within and between atoms, molecules and chemical compounds
- EMR wave-particle duality
- The photoelectric and Compton effects
- EMR-based radiant energy transfer and balancing
- Emission and absorption spectra of light
- Electric and magnetic field interdependency (or duality)
- Electric current flow and capacitor charge storage and discharge
- Semiconductor P-N junctions
- Beta decay and electron capture
- Electron-positron annihilation
- The ionization process during plasma formation
- The formation and constituents of cosmic radiation (Helium, protons neutrinos and gamma radiation)
- Gravity and Gravity waves

The toroidal model for electrons, positrons and preons consist of a torus core of concentrated energy enveloped by less concentrated energy responsible for a surrounding electromagnetic field. The nature of the concentrated core energy within a CES or electron torus is unknown: it could be a liquid-like flow or consist of fast-moving energy strands, vibrating strings or particles. Further research and mathematical modelling is required to determine the most likely form of the concentrated energy and the associated electromagnetic field energy.

Apart from having different chirality, **electrons** and **positrons** have the same structure and electromagnetic characteristics. To date distinction between free electrons and positrons within a host medium has not been possible, probably because there has been no acknowledgement of the existence of positrons within matter. This lack of acknowledgement has caused problems when considering the nature of an electric current, particularly within semiconductors and how a capacitor stores and releases charge, requiring the invocation of fictional positively charged holes and dipoles.

Positrons require considerably more energy to allow them to escape the host medium than do electrons, and thus it is easy to see how historically their presence was missed. Although a bi-product of radiation and pair production, elaborate high energy accelerators are required to extract useful quantities of free positrons (e.g. the desk-top positron generator described in Part 1), and these require technologies that have only become available over the past 15 years or so. The lack of recognition that positrons exist within matter represents a major setback for Science and has led to erroneous theories and assumptions.

There may be subtle differences in the structure of CESs, electrons/positrons and photons that are unique to each, but, for the purposes of this series of papers, they have all been considered to have identical but scaled-up toroidal structures. CESs are the larger and more energetic, and represent **Preons**, the primary energy source from which other energy evolves. CESs are considered to have the ability to accumulate and release energy as part of the energy balancing processes within and between atoms. On the other hand, electrons and positrons are considered to be secondary or derived forms of concentrated bitron energy, which forms (and possibly re-forms) within bitron bonds.

Bitron bonds may be internal to the atom, keeping the nucleon layers apart and providing compressive strength to the nucleus; or external between atoms keeping the ionic counterparts apart and off-setting the pull of offset bonds. Similarly, photons are considered to be derived secondary energy concentrated within by un-bonded in-flow CESs or captured by un-bonded out-flow CESs within an atom and released with increased wavelength as rebound photons.

STEM is based upon a model for the electron, one of the smallest known sub-atomic particles, consisting of a central toroidal core of fast moving concentrated energy, from which, due to a centrifugal effect, energy escapes from its equatorial boundary to form a swirling field of low level electromagnetic energy. This electron model is significantly different to the monopole point charge model of conventional Science, and leads to an atomic model considerably different to the orbital nuclear model.

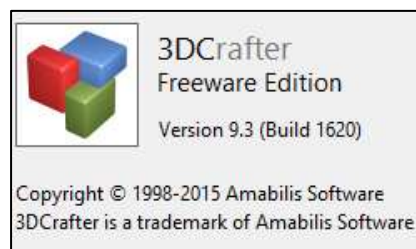
STEM currently does not have a mathematical basis, and has been developed by exploring and explaining as wide a range of Science observations, experiments and theories as possible through internet research: it has been an interesting and challenging learning curve. In its current form STEM provides an excellent framework for future research and detailed mathematical modelling, simulation and testing that has the potential to bring the mathematics of Atomic Physics more in line with Newtonian Physics. It potentially will allow for realistic simulations, working from a micro to a macro model, which should provide better predictive tools than current practices that are geared to the retrospective parameterisation and surface fitting of wave and associated equations to experimental observations.

The five most conjectural aspects of STEM as presented relate to assertions that 1) some bitrons (electron/positron pre-cursors) exist within the nucleus as bitron bonds; 2) positrons are just as important as electrons within matter; 3) electric current is a synchronous 2-way source-to-sink movement of electrons and positrons; 4) the way in which EMR emissions are generated; and 5) Gravity. STEM runs counter to conventional Science beliefs related to the monopole electron and orbital nuclear model which have become an important part of Science culture and education. It challenges many long-held Science beliefs and theories, and herein lies a problem more cultural than scientific.

## Acknowledgements and References

3D Modelling Software

**3DCrafter** by Amabilis Software



Technical References

Most technical detail was obtained from **Wikipedia**



### References (relevant to Parts 1 to 3)

1. Bach R, Pope D, Liou S and Batelaan H : *Controlled double-slit electron diffraction*, New J. Physics, March 2013
2. Bergman D and Wesley J : *Spinning Charge d Ring Model of Electron Yielding Anomalous Magnetic Moment*, Common Sense Science, February 2002
3. Bianchi C and Melon A : *Natural and man-made terrestrial electromagnetic noise*, Annals Of Geophysics, June 2007
4. Bostick W : *Mass, Charge and Current: The Essence and Morphology*, Physics Essays, 1991, v.4(1), 45–59
5. Cambier J and Micheletti D : *Theoretical Analysis of the Electron Spiral Toroid Concept*, NASA, December 2000
6. Clarke B : *'The Quantum Puzzle - Critique of Quantum Theory and Electrodynamics'*, World Scientific, June 2017
7. Consa O : *Helical Solenoid Model of the Electron*, Progress in Physics, Volume 14, Issue 2, April 2018
8. Consa O : *The Helicon - A New Preon Model*, Progress in Physics, Volume 14, Issue 4, October 2018
9. Der-Chi, Chen L, Van Thai N and Ashrai S : *Study of Ag and Au Nanoparticles Synthesized by Arc Discharge in Deionized Water*, Journal of Nanomaterials, Vol 2010 Article 634757
10. Kanarev P : *Particle Resolution*, Proceedings of the NPA, Albuquerque m 2012
11. Kyriakos A : *Geometrical illustration of the electromagnetic representation of Dirac's electron theory*, arXiv:quant-ph/0407071v1, July 2004
12. Lapoint D : *The Primer Fields*, videos at <http://www.rexresearch.com/lapoint/lapoint.htm>
13. Lincoln D : *The Inner Life of Quarks*, Scientific American, November 2012
14. Osmera P : *Fractal Dimension Of Electron*, Proceedings of MENDEL, June 2012
15. Padgett M et Al : *'Photon Orbital Angular Momentum: Generation, measurement and application to QKD'*, Proceedings of SPIE, 2012
16. Sarri G et al : *Table-Top Laser-Based Source of Femtosecond, Collimated, Ultra-relativistic Positron Beams*, Phys. Rev. Lett. 110, 255002, June 2013
17. Shengtao M et Al : *'On-chip discrimination of orbital angular momentum of light with plasmonic nanoslits'*, Nanoscale, Royal Society of Chemistry, 8.2227, 2016
18. Wayte R : *A Model of the Electron*, Progress in Theoretical Physics, July 2010
19. White Paper : *Antenna Patterns and Their Meaning*, Cisco Public Information, 2007
20. Williamson J and Van der Mark M: *Is the Electron a Photon with Toroidal Topology?*, Annales de la Fondation Louis de Broglie, Vol 22, No. 2, 133, 1997
21. Willner M et al : *'Reconfigurable orbital angular momentum and polarization manipulation of 100 Gbit/s QPSK data channels'*, Optics Letters, Vol. 38, No. 24, December, 2013
22. Yao A and Padgett M : *'Orbital angular momentum: origins, behaviour and applications'*, Advances in Optics and Photonics, 3 (2). p.161. ISSN 1943-8206, July 2012
23. Zhang J, Zhang L and Xu W : *Surface plasmon polaritons: Physics and applications*, Journal of Physics, March 2012
24. Zyga L : *'New mirror reflects light differently than conventional mirrors'*, phys.org, November, 2017

# Appendix: Micro and Radio Waves

Micro and radio waves have frequencies less than 300 GHz corresponding to wavelengths from 1 millimetre upwards. Radio and micro waves can be man-made or result from natural sources. Unlike other frequencies in the EMR spectrum, radio and micro waves have the ability to pass through Earth's atmosphere intact (see figure 29): this, plus the ability for data to be encoded and decoded using frequency and amplitude modulation techniques, make them invaluable for communication purposes.

The ability of man-made radio waves to pass through the Earth's atmosphere intact, whereas the rest of the EMR spectrum cannot, does suggest that they could possibly be different in nature to other EMR.

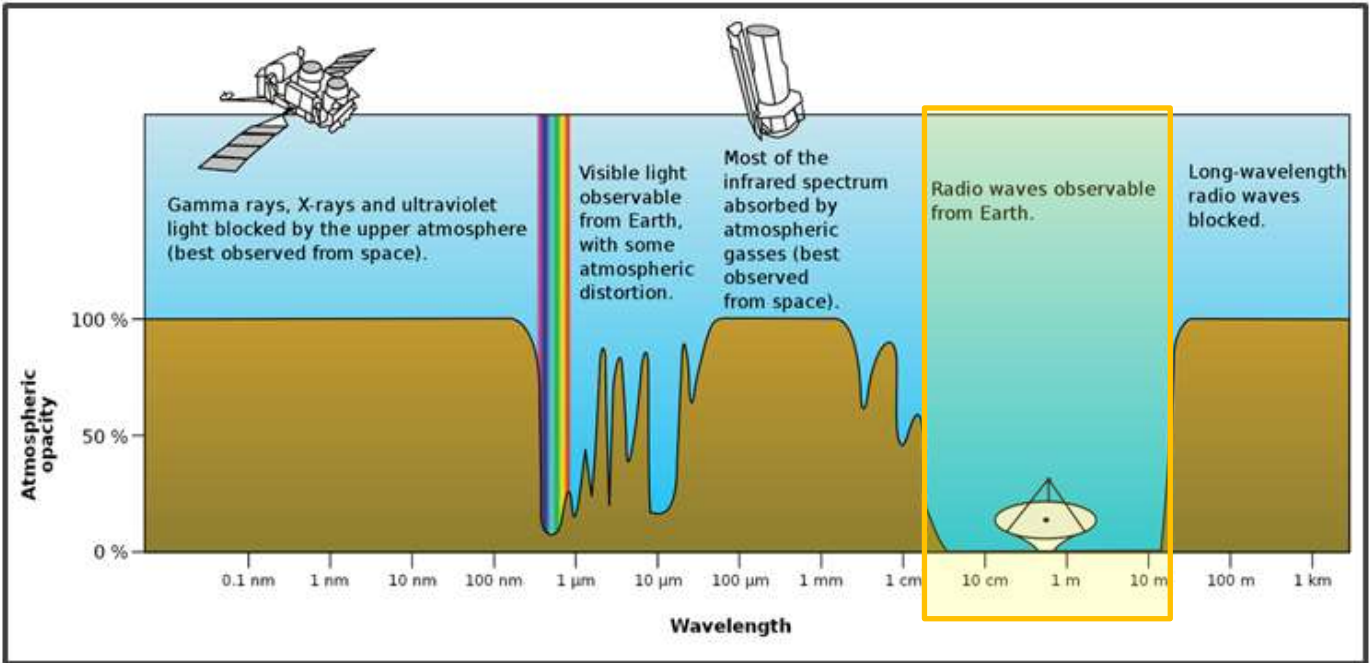


**Figure 29: Electron and Positron Electromagnetic Field Patterns**

Man-made micro and radio waves are generated by a capacitor and inductor loop type of circuitry that delivers an oscillating current to an aerial. It is the oscillation frequency that dictates the frequency of the emitted micro and radio waves. STEM contends that the energy-wave nature of such man-made radio/micro transmission relate to the variation in photon concentration from zero to the maximum concentration in the wave peaks, as shown in figure 30. Although a range of photon wavelengths in the micro/radio wavelength range are transmitted, it is considered to be the photon density within CO and AO-photon concentrations that defines the transmitted wave-form picked up by the receiving aerial. Man-made micro and radio waves are thus formed from EMR photons but are distinctly different to the 'normal' EMR such as light and X-ray radiation.

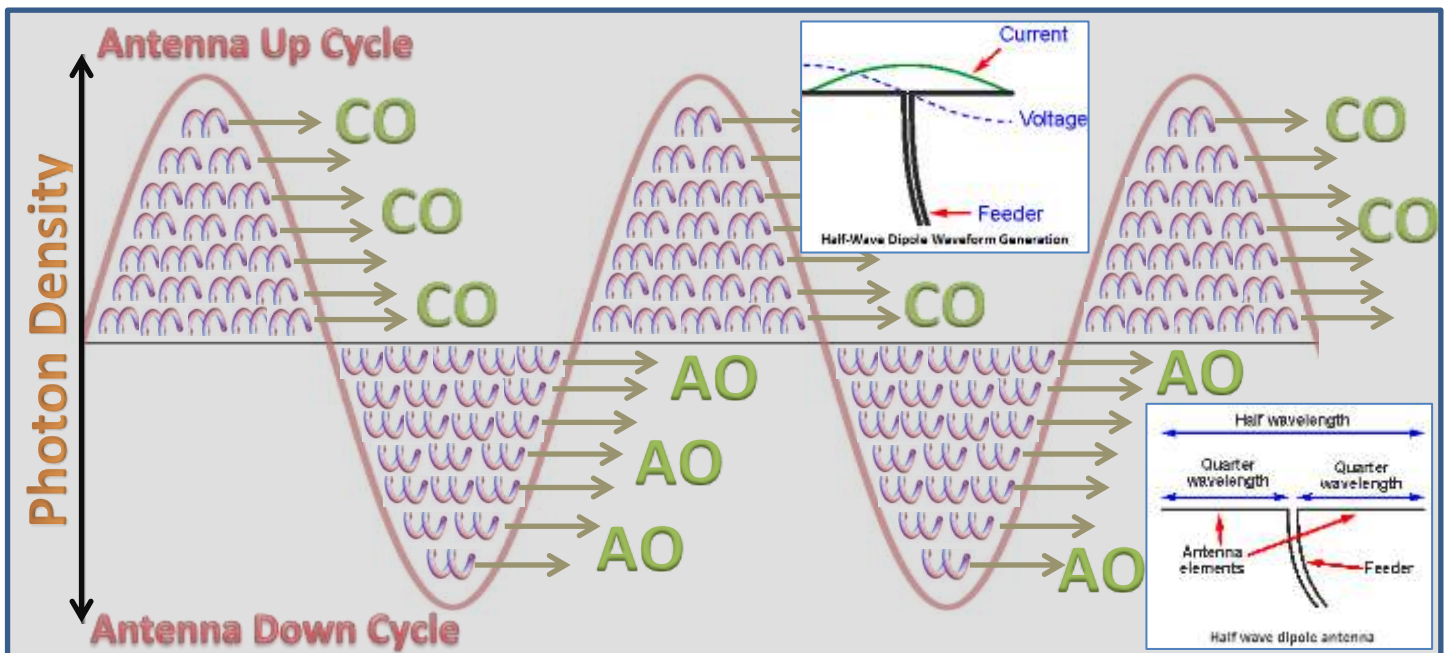


**Figure 30: Man-Made Micro and Radio Waves**

For a hypothetical perfect radio aerial, the transmitted wave fronts would spread as spherical sets of waves and troughs of different photon densities. Larger power transmitters are simply able to pump out more photons per cycle.

In practice, radio antennae display a range of radiation patterns. The radiating radio waves from a dipole antenna consist of electric field half-waves created by an alternating electric current applied to the antenna's two vertical metal rods. The oscillation frequency of the alternating current switches the antenna rod charge between positive (+) and negative (-), producing successive concentration bands of AO and CO-photons (highlighted in red and blue in figure 31): [the related animation](#) clearly shows how the outwardly radiating electric field waves considered to correspond to successive waves of e-photon and p-photon concentrations.

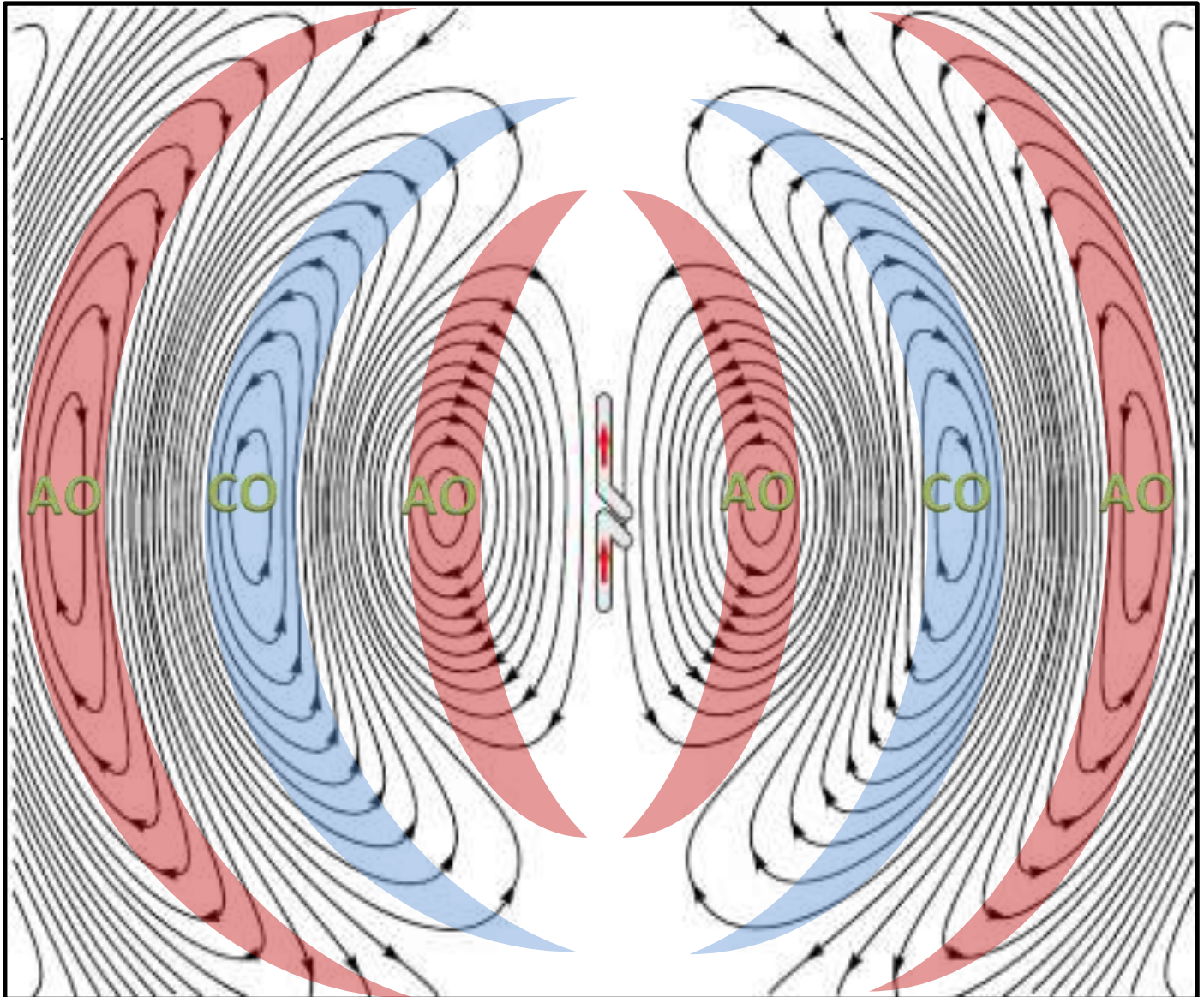


**Figure 31: Electromagnetic Field Patterns for a Dipolar Antenna**

As explained above, man-made micro and radio waves are different to 'normal' EMR: they represent photons that have been concentrated into robust synthetic standing energy-waves that can be modulated to encode data, and which can be received by an appropriately tuned antenna and de-modulated to decode carried data. Apart from technologies using pulsed laser light, data packaging is only possible with man-made EMR in the micro/radio wavelength range: another indication of how different it is to 'normal' EMR.

